THE EFFECTS OF CLOSING ANGLE AND PROXIMITY OF FREE SURFACE ON SEPARATION ON A SUBMERGED BODY OF REVOLUTION

by

CARLOS M. CHARNECO, JR.
Lieutenant, U. S. Navy

and

SAMUEL W. LAYN
Lieutenant, U. S. Navy

SUBMITTED IN PARTIAL FULFILLMENT OF THE REQUIREMENTS FOR THE DEGREE OF NAVAL ENGINEER AND THE DEGREE OF MASTER OF SCIENCE IN NAVAL ARCHITECTURE AND MARINE ENGINEERING.

at the

MASSACHUSETTS INSTITUTE OF TECHNOLOGY

MAY 1962

THE EFFECTS OF CLOSING ANGLE AND PROXIMITY OF FREE SURFACE ON SEPARATION ON A SUBMERGED BODY OF REVOLUTION

BY

CARLOS M. CHARNECO, JR.
Lieutenant, U. S. Navy
B.S., United States Naval Academy
1956

and

SAMUEL W. LAYN
Lieutenant, U. S. Navy
B.S., United States Naval Academy
1955

SUBMITTED IN PARTIAL FULFILLMENT OF THE REQUIREMENTS FOR THE DEGREE OF NAVAL ENGINEER AND THE DEGREE OF MASTER OF SCIENCE IN NAVAL ARCHITECTURE AND MARINE ENGINEERING

at the

MASSACHUSETTS INSTITUTE OF TECHNOLOGY

May 1962

Signature of Authors: _____

Department of Naval Architecture
and Marine Engineering, May 19,1962

Certified by: _____
Thesis Supervisor

Accepted by: _____
Chairman, Departmental Committee
on Graduate Students

THE EFFECTS OF CLOSING ANGLE AND PROXIMITY OF FREE SURFACE ON SEPARATION ON A SUBMERGED BODY OF REVOLUTION

by **CARLOS M. CHARNECO, LT.,USN.,and SAMUEL W. LAYN,LT.,USN.**

Submitted to the Department of Naval Architecture and Marine Engineering on May 19, 1962 in partial fulfillment of the requirements for the Master of Science degree in Naval Architecture and Marine Engineering and the Professional degree of Naval Engineer.

ABSTRACT

This thesis conducts an experimental investigation of the effects on separation of the closing angle of the stern section, the depth of submergence or proximity of the free surface, and the speed of a submerged body of revolution. The results of this investigation are then compared to the results obtained from two existing theoretical criteria for the prediction of the separation point on such bodies in turbulent flow. The point of separation is observed experimentally by photographing dye-flow patterns over the stern of the model at three speeds from .75 to 1.7 knots, at three depths of submergence corresponding to surfaced, near surface and fully submerged conditions for five different body stern shapes increasing in streamlining from a blunt hemisphere to a finely shaped almost pointed section. Equivalent body profiles to the outside of the turbulent boundary layer displacement thickness are computed and potential flow pressure-velocity distributions based upon the equivalent profiles are calculated and used in evaluating the separation criteria.

It is concluded from the results that initiation of separation occurs at a nearly constant body angle on all bodies tested regardless of the degree of streamlining. Experimental results show no apparent effect of depth of submergence on the separation point and the effect of speed shows no clear cut pattern. The sensitivity of the variables used in the separation criterion on the predictions of the separation point are evaluated and recommendations are made for further studies and experimentation.

Thesis Supervisor: Philip Mandel

Title: Associate Professor of Naval Architecture

ACKNOWLEDGMENTS

The authors express appreciation to Professor Mandel for his assistance and motivation. His optimism and enthusiastic interest were a big help.

The model used in this study was constructed and furnished by David W. Taylor Model Basin, Carderock, Maryland. Special thanks are due those staff members who assisted Lt. Charneco in its design and construction during his 1961 summer placement there.

The efforts of Mr. Mike Pearlman, Department of Naval Architecture and Marine Engineering at M.I.T., in assisting the authors at the M.I.T. Ship Model Towing Tank are acknowledged and appreciated.

This work was done in part at the Computation Center at M.I.T.

TABLE OF CONTENTS

LIST OF FIGURES

LIST OF FIGURES (cont'd)

LIST OF TABLES

NOTATION

Symbol	Meaning	Units
C	Non-dimensional coefficients	
E	Error functions	
K	Matrix functions of body	
K^1	Matrix functions of prolate spheroid	
L	Body length	ft. or in.
P	One half the perimeter of the body profile	ft.or in.
R	Gaussian weighting functions	
R_S	Reynold's number, along body profile	
R_X	Reynold's number, along x-axis	
S	Surface area, over body	ft.^{2}or in.^{2}
U	Total velocity along body	ft./sec.
U_∞	Free Stream velocity	ft./sec.
V	Velocity of body	ft./sec.or knots
X	Distance along x-axis	ft.or in.
Y	Distance along y - axis	ft.or in.
ds	Element of arc length along body	
g(x,t)	Function of prolate spheroid whose ends coincide with body ends and intersects body at x = t	
g	Acceleration due to gravity	
k	Matrix functions of body	
k_1	Longitudinal virtual mass coefficient of given body	
$k_1(x)$	Longitudinal virtual mass coefficient of prolate spheroid at x = t	
n	Reciprocal of exponent in boundary layer velocity profile	
k'	Matrix functions of prolate spheroid	

NOTATION (Cont'd)

Symbol	Meaning	Units
p	Dynamic pressure	lb/ft^2
q	Stagnation pressure	lb/ft^2
r	Radius of body profile (calculation for corrected radius)	in.
r	Distance from location of point source on x-axis to point on body profile (calculation of pressure distribution)	in.
t	Location of point source on x-axis, also equal to position of Gaussian abscissae on x-axis, normalized	
u	Component of velocity along x-axis	ft/sec
v	Component of velocity along y-axis	ft/sec
w	Axisymmetric potential function	
x	Distance along x-axis, normalized	
y	Distance along y-axis, normalized	
β	Angle between outward normal to body and x-axis (calculation of pressure distribution)	
β	Constant in separation criterion	
γ	Angle between normal to body and y-axis or between tangent to body and x-axis	
Δ	Ratio of δ^*/δ	
δ	Boundary layer thickness	in.
δ^*	Boundary layer displacement thickness	in.
θ	Boundary layer momentum thickness	in.
λ	Ratio of body length to body diameter	
ν	Kinematic viscosity of water	ft^2/sec

NOTATION (Cont'd)

Symbol	Meaning	Units
ξ	Normalized position of Gaussian abscissae based on body length of 2 and from -1 to + 1	
ρ	Mass density of water	slugs/ft^3
ϕ	Velocity potential function	
ψ	Stokes stream function	
Ω	Ratio of θ/δ in calculation of corrected body profile	
Ω	Stream function of a unit source on the x-axis	

Subscript	Meaning
d	Subscripts drag coefficient
f	Subscripts coefficient of friction
i	Gaussian abscissae index
j	Gaussian abscissae index
k	Velocity is in knots.
n	Refers to direction of body normal in derivation of pressure-velocity distribution
n	Index of iteration for solving equation of pressure-velocity distribution
p	Subscripts pressure coefficient
pl	Quantity referred to flat plate
r	Subscripts residual resistance coefficient
t	Subscripts total drag coefficient
x	Quantity referred to x-axis

I - INTRODUCTION

Separation of turbulent flow with its associated causes and effects has for the last half century been a subject of controversy in the field of naval architecture and ship design. It is in this aspect of fluid flow that the naval architect has his greatest lack of knowledge. There is even considerable debate and controversy as to just what is known and what is not known on the subject of separation, its causes and effects. Little has been mentioned in the past regarding this aspect of fluid flow in references or texts on ship design. What has been stated has been conjecture based on limited theoretical calculations, sketchy experimentation, or recalled experience and observations.

The causes and effects of separation and the parameters relating to them are complicated and closely linked and must be fully understood before any definite design criteria of value can be established for application to ship and submarine forms. Separation of flow on such forms involves the three dimensional boundary layer and turbulence theories which have hardly been more than elaborated because of their associated mathematical difficulties. Even the mathematically simpler axialsymmetric flow becomes involved with the problems of turbulent flow which is not fully understood or theoretically formulated for the relatively

simple case of two dimensional flow over a flat plate.

The ultimate goal is to establish a valid, but simply applied, theoretical criterion to predict the separation point and a foolproof method of testing such a criterion with models to aid naval architects in improving ship design. To do the latter the scaling effects involved in separation must be firmly established and understood as well as understanding the basic phenomenon of separation itself. The most important and difficult step in realizing the formulation of such a criterion is the determination of the significant parameters to be used and the quantitative effect of each on the location of the point of separation. Faired surfaces with modest closing angles apparently retard separation but the limiting magnitude of the body closing angle or extent of fairing required to minimize separation is unknown.

The effects of hydrostatic pressure and atmospheric pressure on separation in general, and in particular the effect on the limiting closing angle have been the subject of considerable debate. Saunders [1]* gives some information relating to these topics but this information has apparently never been checked or verified. The effects of the free surface on separation on a submerged body as it approaches and penetrates the free surface is another area of considerable debate. Body speed and surface roughness are other possible parameters.

* Numbers in brackets refer to works referenced in Appendix H.

The object of this thesis is to investigate the effects on separation of varying depth of submergence or proximity to the free surface, body speed, and the closing angle of the stern of the body. The results are necessarily qualitative in nature since the primary tool used in this investigation, dye-stream photography,is limited in the exactness to which the point of separation can be determined by noting the location of the familiar flow pattern of separation, i.e., abrupt departure of the streamlines of flow from the body surface. Originally it was hoped to relate the observed movement of the separation point, if any, with the independent variation of the parameters listed above to the form drag on the body. However, the results of the drag measurements on the model were unsatisfactory due to faulty or inadequate instrumentation and this could not be done. Two separation criteria , one developed by Stratford [2] and one described by Granville in [3] , are theoretically evaluated and the results compared to the observed point of separation from the dye-stream photographs. This provides some insight as to validity of the criteria and the significance of the parameters used therein.

It is felt that the results of this thesis are a step, although incremental, toward determining what the significant parameters in separation of flow are and how they are related to the phenomenon of separation.

II - PROCEDURE

A. General.

The work presented here was performed in three phases. In the first phase model velocity and drag were measured experimentally and dye-flow photographs were taken of the model stern section for a systematic series of tests. In the second phase theoretical calculations were made to determine the point of separation on the body which could be related to that observed in the photographs. This phase involved the calculation of the turbulent boundary layer displacement and momentum thickness, the pressure-velocity distribution over the resulting corrected body and the use of these quantities in two separation criteria for turbulent flow. The third phase was the analysis of the results of phases one and two to determine and relate, if possible, the effects of the independent variation of speed, depth of submergence, and stern shape on the observed separation point location on the body as well as to compare and relate the observed point to the calculated point of separation.

B. Experimental Phase.

In this phase experiments to visually determine the point of separation on the model and to measure the total drag on the model were conducted at the Massachusetts Institute

of Technology Ship Model Towing Tank under the supervision of the Department of Naval Architecture. Drag and velocity data and dye-flow photographs were obtained for the model at three speeds, at three depths of submergence corresponding to surfaced, near surfaced and submerged conditions, and with five varying shaped tail sections which modified the closing angle of the model's stern.

General Description of Equipment.

Figure I is a sketch of the model showing the variation in stern section and the waterlines of the three depths used. Figure II shows a view of the towing tank and towing carriage, while Figure III shows the carriage control station and instrumentation.

The model, #4893, was constructed at the David Taylor Model Basin, Carderock, Maryland, and is a blunt nosed circular cylinder consisting of three main parts: a blunt solid mahogany nose section, a long hollow aluminum parallel middlebody, which contains the dye system, and five solid mahogany stern sections of varying shape and length. To insure operation in turbulent flow a 1/32 inch diameter trip wire was placed around the nose of the model 2.5 inches from the forward end. The offsets and other characteristics for the model and stern sections are given in Appendix A. Figure IV shows the model components.

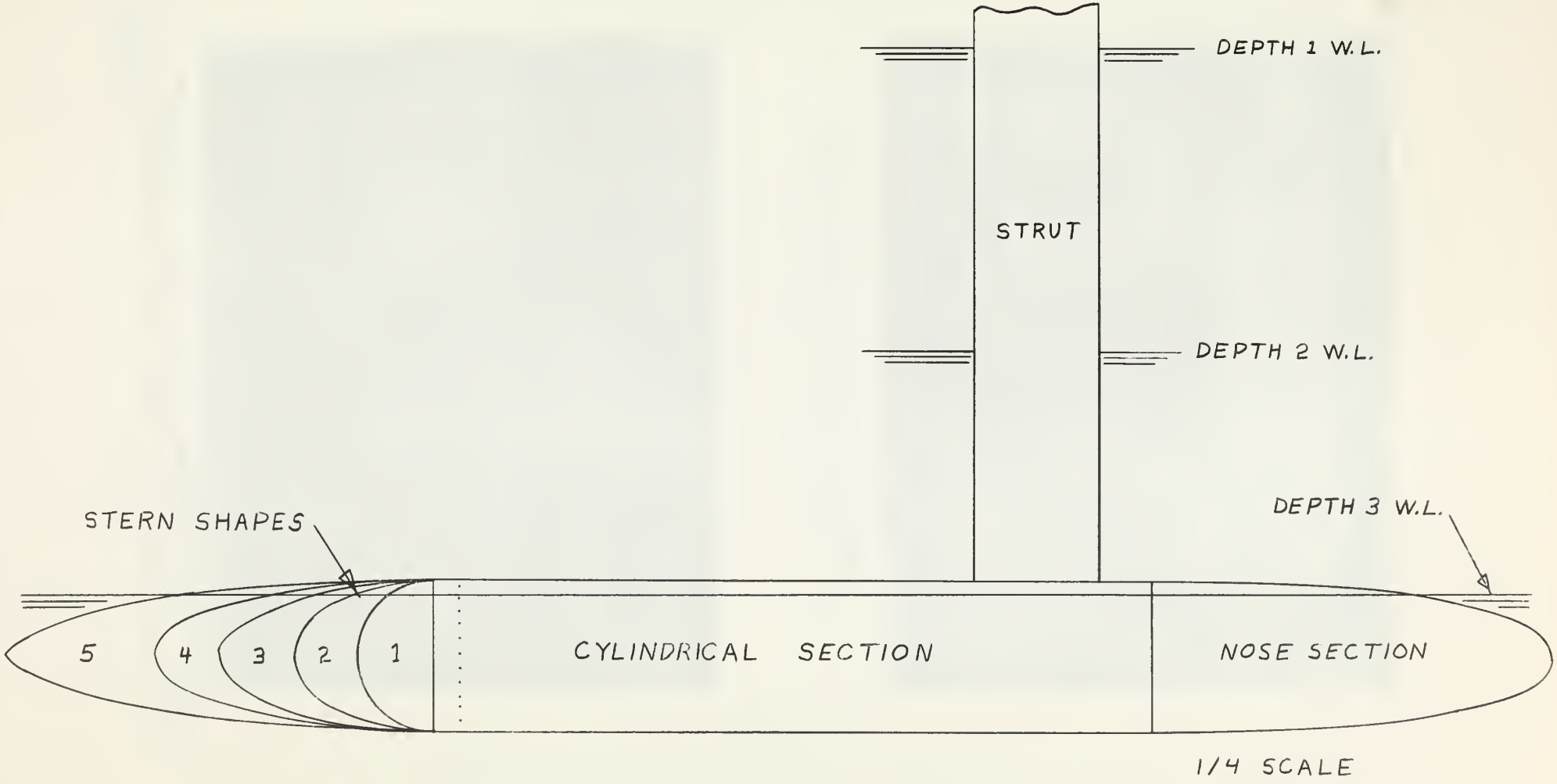

FIGURE I, MODEL AND STERN SHAPES

Figure II - MIT Ship Model Towing Tank

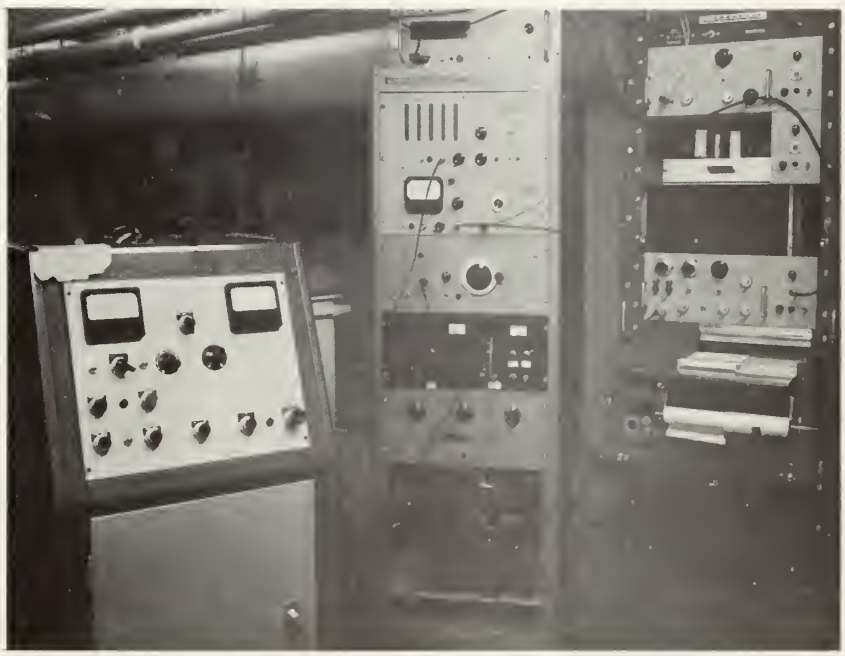

Figure III - Left to right: carriage control console, digital voltmeter and speed measuring equipment, Sandborn recorder.

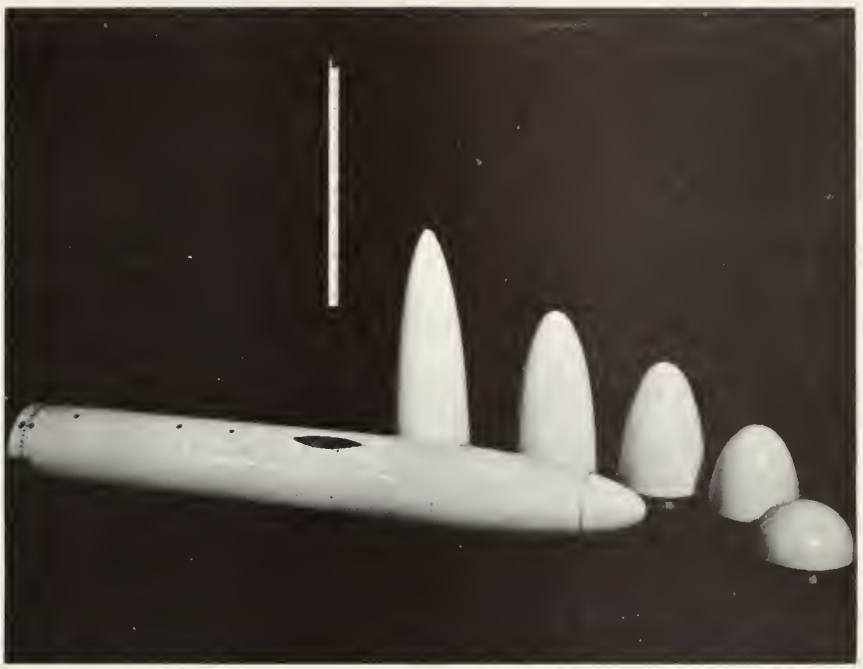

Figure IV - Model and five stern shapes

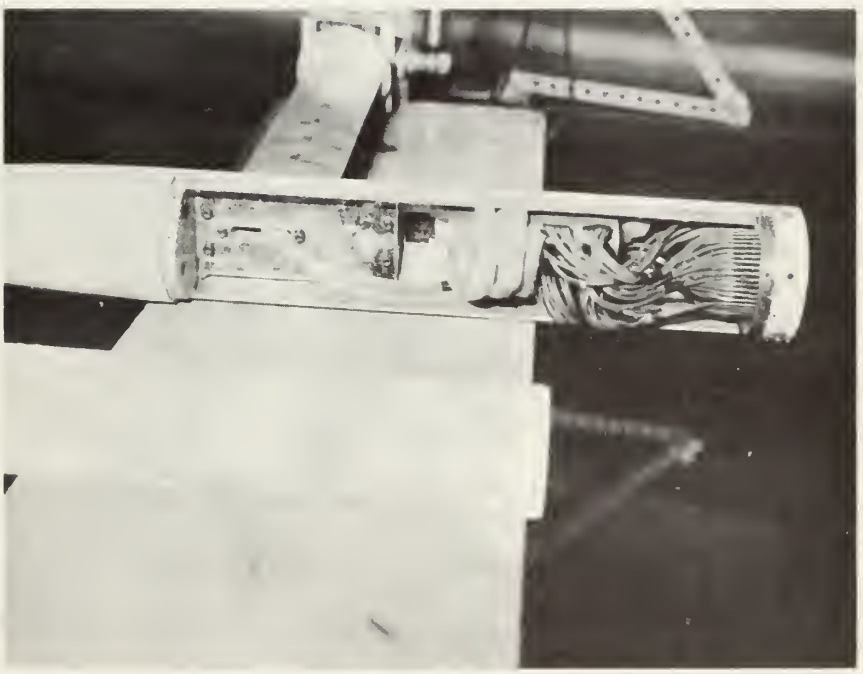

Figure V - Internal view of model parallel middlebody showing support plate, dye tubes, dye manifold and brass dye ring.

The dye system emits dye from 1/16 inch diameter holes spaced every 1/4 inch apart around a circular ring located at the after end of the parallel middlebody. This system is shown in Figure V. Dye was fed to the model from a tank mounted on the towing carriage through 1/4 inch plastic tubing. A solution of water and potassium permanganate was used for dye. Each of the five stern sections can be attached to the model immediately aft of the dye ring. When the model was in motion dye released from the dye ring would stream over the stern section permitting observation of the flow.

The model was rigidly mounted to the towing carriage through a bracket which allowed operation at any depth within the limits of the 18 inch towing street. Figure VI shows the model mounted on the carriage. The towing carriage rides on an overhead rail and is driven by a variable speed electric motor driving a soft rubber wheel in contact with a similar side rail.

Figure VI also shows the drag measuring dynamometer located between the 4:1 ogive towing strut, connected to the model internally, and the $2\frac{1}{2}$ inch diameter hollow-cylinder which was connected to the mounting bracket. The dynamometer measures the axial force between the carriage and the model by means of a differential transformer.

A length of 32 feet was used for each run. The length of run was limited to this length due to a portion of the

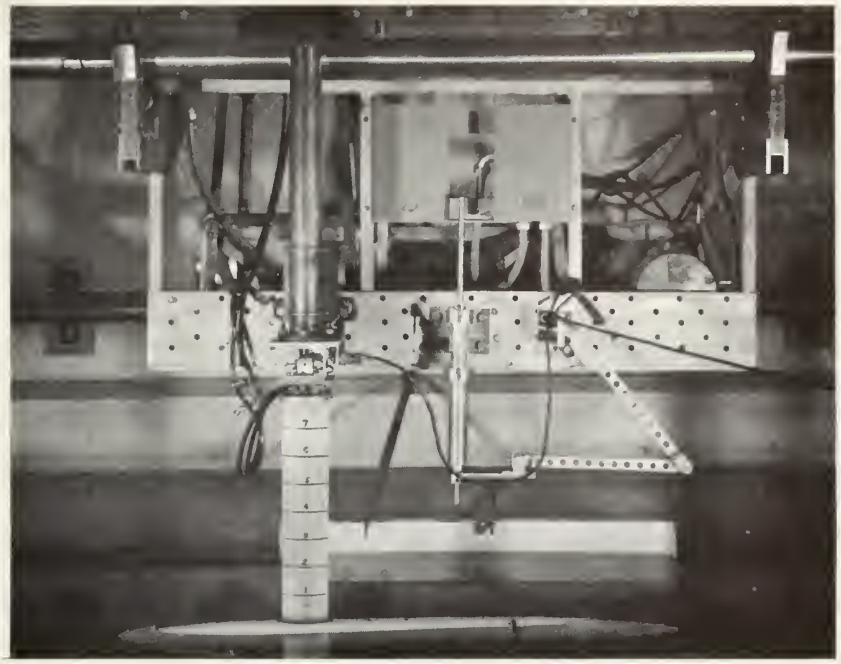

Figure VI - Model mounted on carriage showing towing dynamometer, support bracket, dye tubes and towing strut.

Figure VII - 4x5 view camera and strobe light arrangement at tank window.

carriage rail beyond this length being badly distorted and thereby causing undue carriage vibration. The length of run started at the beach end of the tank and extended to the end of the first of the 10 foot by 4 foot glass windows located in the tank's side wall. A 4x5 view camera was set up at this window along with two high intensity strobe lights which were tripped by the carriage striking a contact on the overhead rail as it reached the proper position in the window near the end of the run. A white, light reflecting, background was installed behind the model because the distance to the far side of the tank was too great to achieve satisfactory exposures. Figure VII shows the photographic set-up that was used. Each stern section was marked at 1/2 inch intervals along its length as an aid in determining the position of separation from the photographs.

The carriage speed was set by the manual speed control dial on the carriage console since the automatic speed control was inoperative. Speed data for each run was recorded on tape with a Sandborn Type 150 recorder and type 1300 preamplifier. Drag force was read out on a type 405 Hewlett Packard D.C. digital voltmeter with input from the type 1100 Sandborn preamplifier. The voltmeter's purpose was to attenuate the high frequency components of the carriage vibrations sensed by the dynamometer as drag fluctuations and to allow a voltage proportional only to model drag to be read out. A more

detailed description of the towing tank and associated equipment, model dye system and dynamometer is given in Appendix B.

Run Procedure

Two runs were conducted for each condition of stern section, depth and speed. On each run a photograph was taken of the dye-flow over the stern section while speed and drag were recorded simultaneously on the Sandborn recorder and digital voltmeter. The tank was allowed to settle between each run. Polaroid pictures were taken occasionally to check exposure and dye-flow definition. Only five of the dye holes in the dye ring were used, two each on the top and the bottom and one on the axis of the body. In turbulent flow the dye present from the other holes tended to obscure the separation point. For laminar flow the use of the entire ring was satisfactory. Figure VIII shows both turbulent and laminar flow. The unused holes were masked off. All screw holes, etc. on the model were filled smooth with a waterproof putty to insure as little flow disturbance as possible.

The model speed was easily obtained from the Sanborn trace and a speed calibration curve; however, the drag could be obtained from the digital voltmeter only by averaging the reading over the run. This was done by recording about ten values of the voltmeter reading during the last third of the run and averaging. This average reading was then compared

A. Laminar flow with all dye holes open.

B. Turbulent flow with all dye holes open.

C. Turbulent flow with only top, bottom and side open.

Figure VIII - Laminar and Turbulent Zone Dye-flow.

0.78 kts.

1.21 kts.

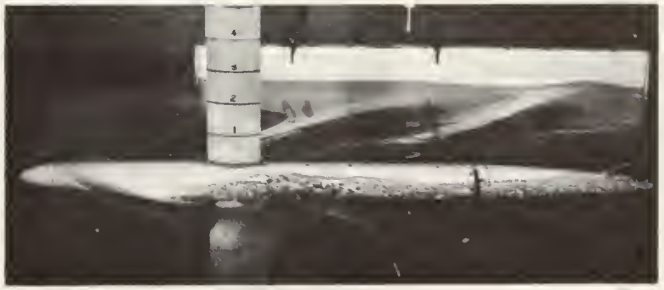

1.58 kts.

Figure IX - Surfaced Bow Waves

to the "zero" drag reading taken prior to each run to determine a voltage difference reading proportional to drag. A calibration curve was determined by applying a known static load to the model and observing the voltmeter reading. Using this curve and the voltage difference reading drag force was obtained.**

C. Theoretical Phase.

In this phase a theoretical position of separation on the body was established after correcting the body for the effects of boundary layer growth. Throughout this phase it was assumed that the flow was turbulent from the nose of the body and that the 1/7 power law holds for the velocity distribution within the turbulent boundary layers.

Calculation of Turbulent Boundary Layer Characteristics.

As indicated in the general discussion of the procedure the value of the displacement thickness on the body and momentum thickness on the body are necessary. Eckert [4] has evaluated the effects of transverse curvature on the turbulent boundary layer on a circular cylinder in compressible flow. These effects are the same as reported by Yu [5] and Landweber [6], which are:

** The drag measurements were unsatisfactory. Appendix E has a more detailed discussion relating to these measurements.

(1) Boundary layer thickness and displacement thickness are less than on the flat plate.
(2) Momentum thickness and local and mean skin friction coefficients are higher than flat plate values.
(3) The effects of (1) occur when the ratio of $\delta/r \approx 0.1$.
(4) The friction coefficients deviate from flat plate values only when ratio $\delta/r \approx 1.0$.

Eckert develops simple equations which relate the value of δ, δ^*, and Θ on the body to values of the same parameters on a flat plate. The assumption is made that the velocity profile within the boundary layer conforms to the 1/7th power law distribution of $\frac{U}{U_\infty} = \left(\frac{Y}{\delta}\right)^{1/7}$ and that Blasius' Law relating wall shear stress as inversly proportional to the fourth root of the boundary layer thickness are uneffected by the curvature. The assumption is also made that the boundary layer is turbulent from the beginning and it starts from the nose of the body with zero thickness.

The relationships developed for incompressible flow are given below and the reader is referred to [4] for the derivation details which are straightforward.

Relationship for boundary layer thickness

$$\frac{\delta}{\delta_{pl}} = \left(\frac{1}{1+\delta/3r}\right)^{4/5} \qquad (1)$$

where,

$$\delta_{pl} = \frac{0.38\ X}{(Rx)^{0.2}} \qquad (1a)$$

Although (1) is implicit in δ it can be easily solved by using δ_{pl} as a first try and iterating the results.

Relationships for Displacement thickness.

$$\frac{\delta^*}{\delta^*_{pl}} = \frac{1 + \frac{\delta}{r} - \sqrt{1 + \frac{2\delta}{r}\left(1 - \Delta_{n_{pl}}\right) + \frac{\delta^2}{r^2}\left(1 - \Delta_{2n_{pl}}\right)}}{\frac{\delta}{r}\,\Delta_{n\,pl}\left(1 + \frac{\delta}{3r}\right)^{4/5}} \qquad (2)$$

where,

$$\Delta_{n\,pl} = \frac{\delta^*_{pl}}{\delta_{pl}} = \frac{1}{n+1} \qquad (2a) \qquad \delta^*_{pl} = \frac{\delta_{pl}}{1+n} \qquad (2b)$$

$$\Delta_{2n_{pl}} = \Delta_{n_{pl}} \frac{(n+1)}{(2n+1)} = \frac{1}{2n+1} \qquad (2c) \qquad \frac{u}{u_\infty} = \left(\frac{y}{\delta}\right)^{\frac{1}{n}}$$

Relationships for Momentum thickness.

$$\theta = \delta\left(\Omega_{n\,pl} + \frac{\delta}{2r}\,\Omega_{2n\,pl}\right) \qquad (3)$$

where,

$$\Omega_{n_{pl}} = \frac{n}{n+1} - \frac{n}{n+2} = \frac{n}{n+1(n+2)} = \frac{\theta_{pl}}{\delta_{pl}} \qquad (3a)$$

$$\Omega_{2n_{pl}} = \Omega_{n_{pl}} \frac{(n+2)}{(n+1)} = \frac{n}{(n+1)(2n+1)} \qquad (3b)$$

The value of δ^* calculated from (2) was applied as a correction to the body surface after the manner described in [7] as is shown in Figure X taken from [7].

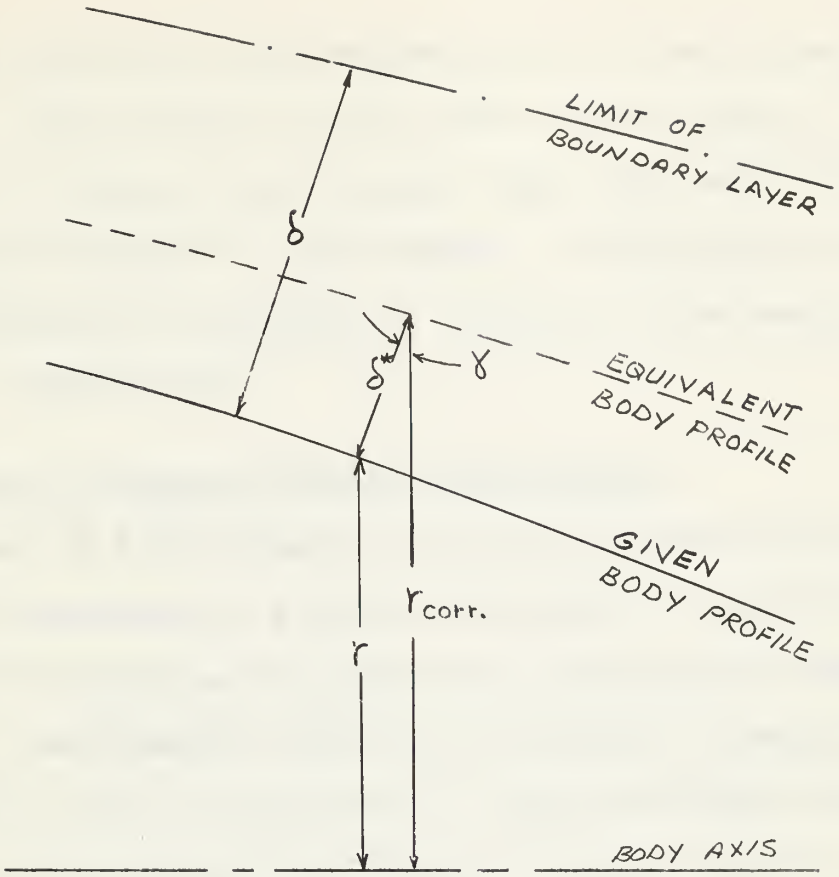

Figure X - Equivalent Body Profile with Displacement Thickness

Thus the corrected body will have a radius given by

$$r_{corr} = r + \cos \gamma \, \delta^* \qquad (4)$$

For use in the calculation of the pressure velocity distribution discussed in the next section this radius was normalized as follows:

$$r_{\underset{norm}{corr}} = \frac{r_{corr}}{\text{body length}/2} \qquad (4a)$$

An IBM 7090 computer program, Program II, was written to evaluate equations (1,2,3,4 & 4a) at 16 points on each of the 5 bodies for 9 speeds. These 16 points correspond to the location of the 16 ordinates required for the Gaussian 16 point

quadrature rule use in the determination of the pressure velocity profile. The values of body radius and the angle θ were picked off at each of the 16 points from full scale drawings of the 5 bodies prepared by the authors. A tabulation of this data is contained in Appendix A. Details of the computer program are in Appendix C.

Calculation of Pressure Velocity Distribution

Potential Flow Pressure and Velocity Distribution was calculated according to a method developed by Landweber [8]. Two types of solutions are given for obtaining the steady, irrotational, axisymmetric flow of an inviscid, incompressible fluid about a body of revolution. The first method involves an iterative type solution for Fredholm integral equation of the first kind and is not used in this work. The second method obtains the velocity directly as the exact solution of an integral equation of the first kind by an arithmetic procedure. Using the second method as outlined in [8] the basic problem is to solve for the velocity potential ϕ which is dependent on x, y and satisfies Laplace's equation in cylindrical coordinates:

$$\frac{\partial}{\partial x}\left(y\frac{\partial \phi}{\partial x}\right)+\frac{\partial}{\partial y}\left(y\frac{\partial \phi}{\partial y}\right)=0 \qquad (5)$$

where the equation of the normalized body profile is in the form: $y^2 = f(x)$ (Figure XI shows method of normalizing the body)

and $u = -\frac{\partial \phi}{\partial x}$, $v = -\frac{\partial \phi}{\partial y}$

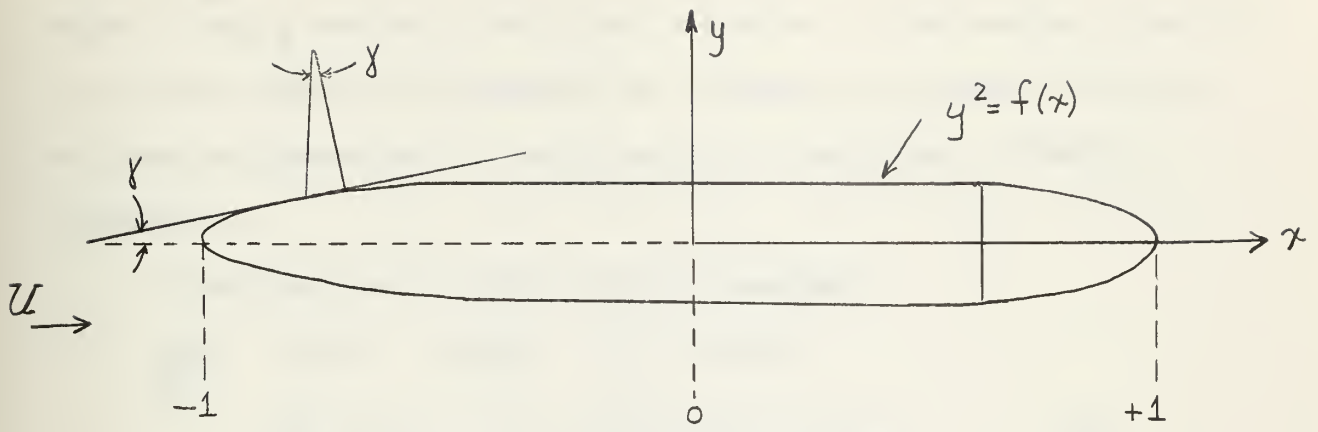

Figure XI - Normalized Body Profile

There also exists a Stokes stream function $\psi(x,y)$ which satisfied the equation:

$$\frac{\partial^2 \psi}{\partial x^2} + \frac{\partial^2 \psi}{\partial y^2} = \frac{1}{y} \frac{\partial \psi}{\partial y} \qquad (6)$$

For uniform flow of velocity U parallel to the x-axis

$\phi = -Ux$ and $\psi = -\frac{1}{2} U y^2$ at infinity

The following boundary condition on the body must also be satisfied:

$$\left(\frac{\partial \phi}{\partial n}\right)_s = -V \cos \beta$$

Where V = velocity of the body and β = the angle between the outward normal to the body and the x-axis.

Derived from Green's Theorem the equation:

$$\iint \phi \frac{dw}{dn} \, dS = \iint w \frac{d\phi}{dn} \, dS \qquad (7)$$

where ϕ and w are any functions harmonic in the region exterior to a given body and vanishing at infinity, is used to obtain an integral equation for axisymmetric flow about a body of revolution.

Substitution of: $dS = 2\pi\, y\, ds$ and

$\frac{d\phi}{dn} = -\sin\gamma$ into (7) gives:

$$\int_0^P y\phi \frac{dw}{dn}\, ds = -\int_0^P y\, w \sin\gamma\, ds \qquad (8)$$

y = ordinate of meridian section of the body which is moving in the negative x - direction with unit velocity.

ds = element of arc length along body

γ = angle of the tangent to the body with x - axis

2P = perimeter of a meridian section

With W as an axisymmetric potential function and $\psi(x,y)$ the corresponding stream function

$$y \frac{dw}{dn} = \frac{d\psi}{ds}$$

and $$\int_0^P y\phi \frac{dw}{dn}\, ds = \phi\psi\Big|_0^P - \int_0^P \psi \frac{d\phi}{ds}\, ds$$

If U is total velocity along a body when a stream of unit velocity is superposed in the positive x - direction

$$U = -\frac{d\phi}{ds} + \cos\gamma$$

Since $dx = ds\cos\gamma$ and $dy = ds\sin\gamma$ equation (8) can be written as:

$$\int_0^P U\psi\, ds = \int_0^P (\psi\, dx - yw\, dy) - \phi\psi \Big|_0^P \qquad (9)$$

but $y = \frac{\partial w}{\partial x} = -\frac{\partial \psi}{\partial y}$ since w and ψ are corresponding potential and stream functions and $\psi\, dx - yw dy$ is an exact differential defining a function Ω (x,y) such that

$$\frac{\partial \Omega}{\partial x} = \psi \qquad \frac{\partial \Omega}{\partial y} = -\, y\, w$$

From this and $y \frac{\partial w}{\partial y} = \frac{\partial \psi}{\partial x}$ we obtain

$$\frac{\partial^2 \Omega}{\partial x^2} + \frac{\partial^2 \Omega}{\partial y^2} + \frac{1}{y} \frac{\partial \Omega}{\partial y}$$

which is identical to (6) and is the equation satisfied by Stokes stream function. It can also be verified that w and ψ are corresponding axisymmetric potential and stream functions which satisfy the equation: $\frac{\partial \psi}{\partial x} = -\, y \frac{\partial \phi}{\partial y}$, $\frac{\partial \psi}{\partial y} = y \frac{\partial \phi}{\partial x}$

Writing (9) in terms of Ω

$$\int_0^P U \frac{\partial \Omega}{\partial x}\, ds = \left(\Omega - \phi \frac{\partial \Omega}{\partial x}\right)\Big|_0^P \qquad (10)$$

If Ω is the stream function of a point source of unit strength situated at x = t on the x - axis

$$\Omega = -1 + \frac{x-t}{r} \quad , \quad r = \left[(x-t)^2 + y^2\right]^{\frac{1}{2}} \qquad (11)$$

Then $\frac{\partial \Omega}{\partial x} = \frac{y^2}{r^3}$, and if y vanishes at both limits,

$$\left(\Omega - \phi \frac{\partial \Omega}{\partial x}\right)\Big|_0^P = 2$$

(11) now becomes:

$$\int_o^P \frac{U(x) y^2(x)\, ds}{2\pi^3} = 1 \qquad (12)$$

which is an integral equation of the first kind in which the unknown function is $U(x)$ and the kernel is $y^2/2\pi^3$. When U is determined the pressure distribution is given from Bernoulli's equation;

$$\frac{p}{q} = 1 - (u^2 + v^2) = 1 - U^2$$

where q is the stagnation pressure.

Landweber uses an iteration procedure to solve (12) as follows:

If the iterations are expressed in terms of error functions $E_n(t)$ at the point $x = t$, first obtain $E_1(t)$ from $E_n(t) = 1 - \int_o^P \frac{U_n(x)\, y^2(x)}{2\pi^3}\, ds$

by using the first approximation $U_1(t) = (1+k_1)\cos\gamma(x)$ where k_1 = longitudinal virtual mass coefficient. Then successive iteration $E_2, E_3 \ldots\ldots E_n$ are obtained from

$$E_{n+1}(t) = E_n(t) - \tfrac{1}{2}\int_{x_o}^{x_1} \frac{E_n(x)\, y^2(x)}{x}\, dx$$

where x_o, x_1 are nose and tail abscissæ of the body and finally $U_{n+1}(t)$ is obtained from

$$U_{n+1}(t) = U_1(t) + \cos\gamma(t) \sum_{i=1}^{n} E_i(t) \qquad (13)$$

To evaluate integrals of the form

$$\int_{x_0}^{x_1} \frac{E(x)\, y^2(x)}{\mathcal{M}^3}$$

use $$k(x,t) = \frac{f(x)}{\left[(x-t)^2 + f(x)\right]^{3/2}} \tag{14}$$

$$k'(x,t) = \frac{g(x,t)}{\left[(x-t)^2 + g(x)\right]^{3/2}} \tag{15}$$

where $y^2 = f(x)$ is the equation of the given body profile and $y^2 = g(x, t))$ is the equation of the prolate spheroid whose ends coincide with the ends of the given body, and which intersects the body at $x = t$, i.e.,

$$g(x, t) = f(t)\, \frac{(x-x_0)(x_1 - x)}{(t - x_0)(x_1 - t)} \tag{16}$$

For the spheroid the length - diameter ratio λ is given by

$$\lambda^2 = \frac{(t - x_0)(x_1 - t)}{f(t)} \tag{17}$$

and from this the virtual mass coefficient $k_1(t)$ can be obtained from:

$$k_1 = \frac{\lambda \ln(\lambda + \sqrt{\lambda^2 - 1}) - \sqrt{\lambda^2 - 1}}{\lambda^2 \sqrt{\lambda^2 - 1} - \lambda \ln(\lambda + \sqrt{\lambda^2 - 1})} \tag{18}$$

$E_1(t)$ is then obtained from

$$E_1(t) = 1 - \frac{1+k_1}{2} \int_{x_0}^{x_1} \left[k(x,t) - k'(x,t)\right] dx - \frac{1 + k_1}{1 + k_1(t)} \tag{19}$$

and finally

$$E_{n+1}(t) = \frac{E(t) + k_1}{1 + k} E_n(t) - \frac{1}{2} \int_{x_0}^{x_1} k(x, t) \left[E_n(x) - E_n(t)\right] dx \tag{20}$$

In using Landweber's method the velocity is obtained at 16 points along a body, from t = -1 to t = + 1, corresponding to the Gaussian values (ξ_i) for the 16-point guadrature rule. In applying the rule the integrands in (19) and (20) are evaluated at the 16 Gaussian abscissae $X_j = \xi_j$ for each of the 16 values of $t_i = \xi_i$. Gaussian weighting functions are used to obtain $K_{j\,i} = R_j\, k\,(X_j, t_i)$ and $K'_{j\,i} = R_j k\,(X_j, t_i)$ which are used in evaluating (19) and (20). $U_n(t)$ is then given by (13) and P/q by Bernoulli's equation in the form $P/q = 1 - U_n^2$.

In the application of Landweber's method of determining the pressure-velocity distribution on a body of revolution to the models used in this thesis the corrected body profile as calculated in the previous section was used. The function $Y^2 = f(x)$ for the normalized corrected body profile was not determined because even if it is determined the end result is still a point-wise distribution of U/U_∞ . Instead of determining the polynomial describing the body profile the values of the normalized corrected body radius at each Gaussian ordinant computed in Program II were used. The angle, γ , was again determined from full scale drawings of the model and stern sections.

An IBM 7090 computer program, Program III, was written to determine the pressure-velocity distribution on the body corrected for boundary layer effects using Landweber's method. The program calculates C_p, U/U_∞, absolute velocity and gage pressure on the body at 16 points on each of 5 bodies for 3 different

speeds at each of 3 different depths of submergence. The 9 speeds used are the same as those used in Program II and are the average of the speeds listed for each run and its duplicate, i.e., Run 1 and Run 1A, in the tabulation of experimental data in Appendix D. Thus the outputs of the two programs are a compatible package for application in the separation criterion to be evaluated. This output is in turn compatible with the dye-flow photographs since the same conditions apply. A test solution for Program III was run on the example worked out in [7].

Separation Criteria .

Stratford [2] has developed a rapid method for the prediction of flow separation in turbulent flow from an approximate solution of the equations of motion. The equations are integrated by a modified "inner and outer layer solution" technique developed by Stratford in 1954 for laminar flow boundary layers. The final solution is given by equations (21) through (24) which relate X, Cp, and dCp/dX at the separation position and may be applied to any given pressure distribution. The algebra and procedure for obtaining the separation condition are clearly detailed in [2] and only the results will be given here.

The resulting implicit equation for the separation po-

sition, X, is

$$(2Cp)^{\frac{1}{4}(n-2)} \left(X \frac{dCp}{dx} \right)^{\frac{1}{2}} = 1.06 \beta (10^{-6} Rs)^{-\frac{1}{10}} \quad (21)$$

for $Cp \leq \frac{n-2}{n+1}$

Where: R_s is the Reynolds number based on value of distance X and freestream velocity, Uoo.

$$n = \log 10 \, R_s \quad (22)$$

and $\beta = 0.66$ for $\frac{d^2p}{dX^2} < 0$ (23)

$$\beta = 0.73 \text{ for } \frac{d^2p}{dX^2} \geqq 0 \quad (24)$$

with the resultant value of $\frac{d^2p}{dX^2}$ being that immediately prior to separation. This formulation has a range of uncertainty of 10% due to its inability to fully account for d^2p/dX in the case of turbulent boundary layers. However, the rapidity of the method makes this range of uncertainly acceptable in this case. Granville in [3] has brought forward another even simpler separation criterion It was apparently originally developed by Buri in 1931 at Zurich. The criterion states that separation will occur if the following relation holds:

$$\frac{\theta}{u} \times \frac{Uoo}{L} \times \frac{du}{dX} \times \frac{L}{Uoo} \leqq -0.006 \quad (25)$$

Where: θ = momentum thickness on the body at separation point (Calculated using equation (3)) and L = body length.

since L and Uoo are constants for each body at a particular speed

$$\frac{du}{dx} = \frac{d\left(\frac{U}{Uoo}\right)}{d\left(\frac{X}{L}\right)} \times \frac{Uoo}{L}$$

Equation (25) can thus be written

$$\theta \times \frac{X}{L} \times \frac{U_\infty}{U} \times \frac{d\left(\frac{U}{U_\infty}\right)}{d\left(\frac{X}{L}\right)} \leq -0.006 \qquad (26)$$

Unfortunately the information regarding this criterion is limited to that obtained by the writers from Course 13.012 in the Department of Naval Architecture at M.I.T. and the meager yet reliable reference to it in [3]. A range of uncertainty for the criterion is not known. It is intended to be used as a criterion to be used in scaling separation from model to ship scale.

With the velocity profiles, pressure coefficients, and momentum thickness values on the body determined as outlined in the previous sections it is possible to evaluate both of these criteria and see how they will compare with the experimentally observed points of separation. This was done by hand calculation for a few cases. Sample calculations are given in Appendix F. The results of such calcuations are in the RESULTS section of this thesis.

D. Analysis Phase.

The data obtained from the experimental phase relating to drag was analyzed by utilizing an IBM 7090 computer program, Program I, to reduce the data to coefficient form. The details of this computer program are given in Appendix C. The analysis of the experimental drag data contained in Table D-I of Appendix D showed the data to be unreliable and faulty. Appendix E contains some of the results obtained from the computer program

and a discussion relating to these results. The second step in analyzing the experimental data was to study the dye-flow photographs and determine from them the point of separation and the body angles with respect to the body axis at the point of separation. The point where the dye-flow appeared to abruptly depart from the body profile was taken to be that of the point of separation. Only the flow along the keel of the model was used in determining the location of the point of separation because it was felt that the presence of the towing strut forward would influence the flow over the top of the model. The authors each made independent determinations of the separation position on each run. Differences which arose in interpreting the location of the separation point were then compromised. The determinations were also made prior to the calculation of the separation position from the two separation criteria so that the location of these theoretical points would not influence the interpretation of the photographs. In this manner it was felt that as high as possible degree of precision would be obtained in interpreting the photographs. There was, as was to be expected, considerable judgment involved in establishing the separation point in several of the pictures. A sampling of typical photographs from which the separation point was determined is shown in Figure XII. The location of the observed separation point for each run is contained in Table D2 in Appendix D. The angle between the body

Run 1

Run 2

Run 3

Run 4

Run 5A

Run 6

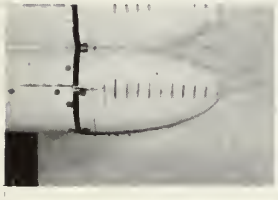

Run 7

Run 8

Run 9A

A. Sequence of Runs on Body 3.

Run 13A
Body 1

Run 12A
Body 1

Run 29
Body 4

Run 20A
Body 2

Run 35A
Body 4

Run 38A
Body 5

B. Runs on Other Bodies.

Figure XII - Typical Dye-flow Photographs

surface and the body axis at the point of separation was determined graphically by plotting the separation point location on full scale drawings of the bodies. The movements of the point of separation were analyzed to see what, if any, correlation could be made between these movements and changes of speed, depth of submergence or body shape. The angle at which separation occurred was similarly analyzed.

The third step in the analysis was to calculate the point of separation by each of the two separation criteria using the results of computer programs I and II. Samples of the output from these programs are contained in Appendix G. Sample calculations for each of the criteria are given in Appendix F. During these calculations the criticality of the various parameters in the criteria were noted. The results of these calculations were compared to the observed point of separation noting location and angle of body surface at the point of predicted separation.

III RESULTS

The results of the procedures described in the previous sections are presented in this section. These results are discussed and conclusions are drawn from them in the next section of the thesis.

The results are presented primarily in graphical form. Figures XIII through XVII show the relationship between the pressure-velocity distribution over the body and the location of the observed separation points. Figures XVIII through XXII show the location of the experimental and calculated points of separation. The body profiles corrected for boundary layer effects are also shown here. Table I contains a breakdown of the experimentally observed separation points on each body by depth of submergence, and speed. The body angle at separation is also shown.

TABLE I

Results of Studies of Dye Flow Photographs and Separation Criteria

Code	BODY #1 Angle	X/L	Points (Speed-Depth)
A	24°	.962	5 @ LM, 2 @ LD, 2 @ MD, 2 @ LS
B	32°	.970	3 @ MM, 2 @ HM, 1 @ MS
C	42°	.978	2 @ HD, 2 @ HS, 2 @ MS
E	6°	.943	BURI CRITERION
F	47°	.982	STRATFORD CRITERION

Code	BODY #2 Angle	X/L	Points (Speed-Depth)
A	25°	.967	1 @ LD, 1 @ LM
B	30°	.976	2 @ MM, 1 @ HM, 1 @ LD, 2 @ LS
C	36°	.983	2 @ MD, 1 @ HD, 1 @ MS, 1 @ LM
D	42°	.989	2 @ HS, 1 @ MS
E	13°	.930	BURI CRITERION
F	38°	.986	STRATFORD CRITERION

Code	BODY #3 Angle	X/L	Points (Speed - Depth)
A	23°	.967	2 @ MS, 2 @ LS, 1 @ HS
B	28°	.975	2 @ LM, 2 @ MM, 1 @ HM, 1 @ HS
C	33°	.982	2 @ HD, 2 @ MD, 2 @ LD 1 @ HM
E	10°	.905	BURI CRITERION
F	46°	.992	STRATFORD CRITERION

Code	BODY #4 Angle	X/L	Points (Speed - Depth)
A	28°	.983	2 @ LD, 1 @ MD
B	38°	.990	2 @ LS, 2 @ MS, 1 @ HD, 1 @ MD, 1 @ LM
C	49°	.996	2 @ HM, 2 @ MM, 2 @ HS, 1 @ LM
E	6°	.881	BURI CRITERION
F	36°	.989	STRATFORD CRITERION

Code	BODY #5 Angle	X/L	Points (Speed-Depth)
A	23°	.978	All speeds at deep depth
B	30°	.988	All speeds at medium depth
C	60°	.998	All speeds at surface
E	5°	.831	BURI CRITERION
F	23°	.979	STRATFORD CRITERION

Separation points are plotted on body profiles in figures XVIII through XXII.

Point designations are the same as outlined in Table D-II of Appendix D; e.g. 2 @ HM means two points were plotted at that location and angle on the body corresponding to two runs at the high speed - medium depth condition.

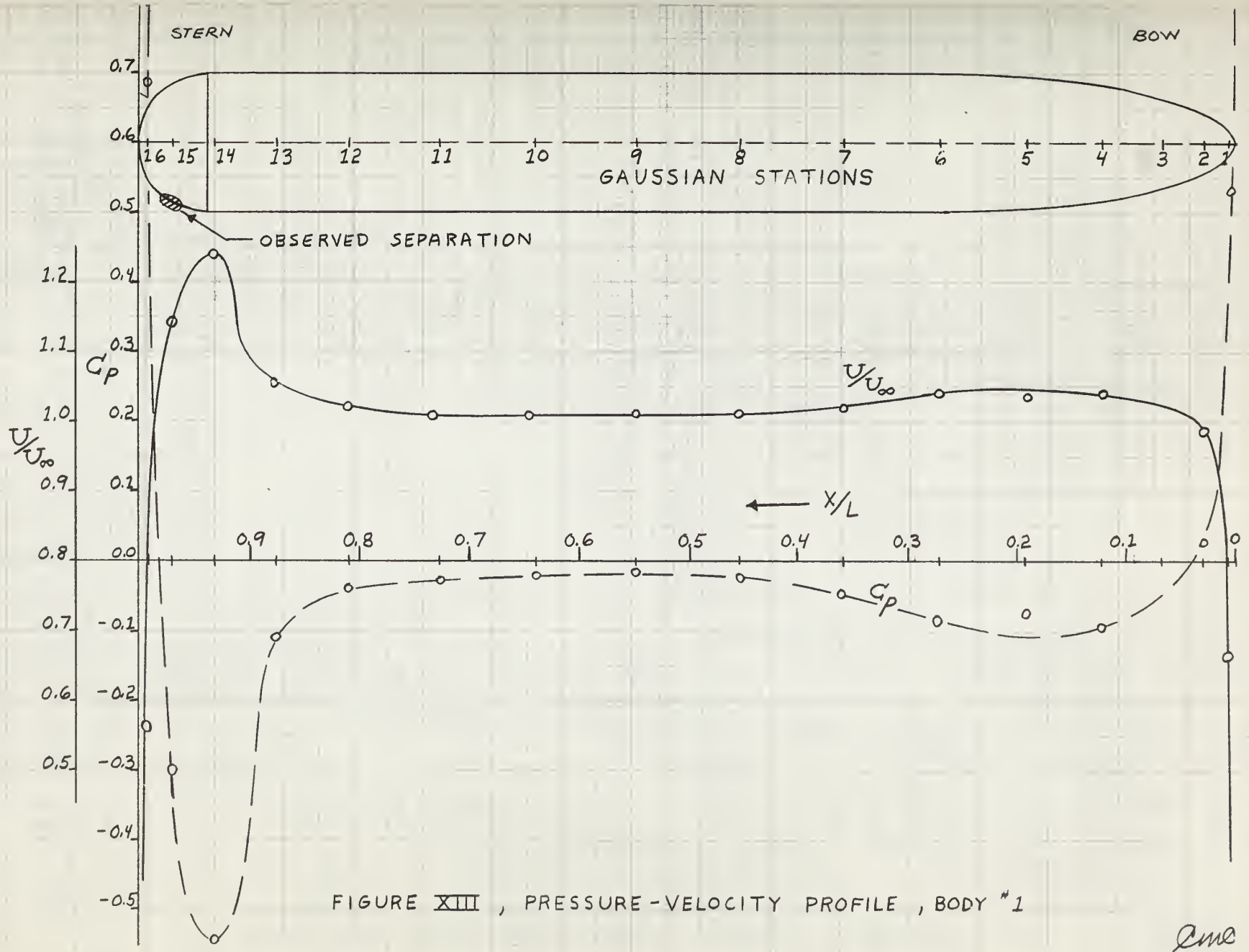

FIGURE XIII , PRESSURE-VELOCITY PROFILE , BODY #1

4/25/62

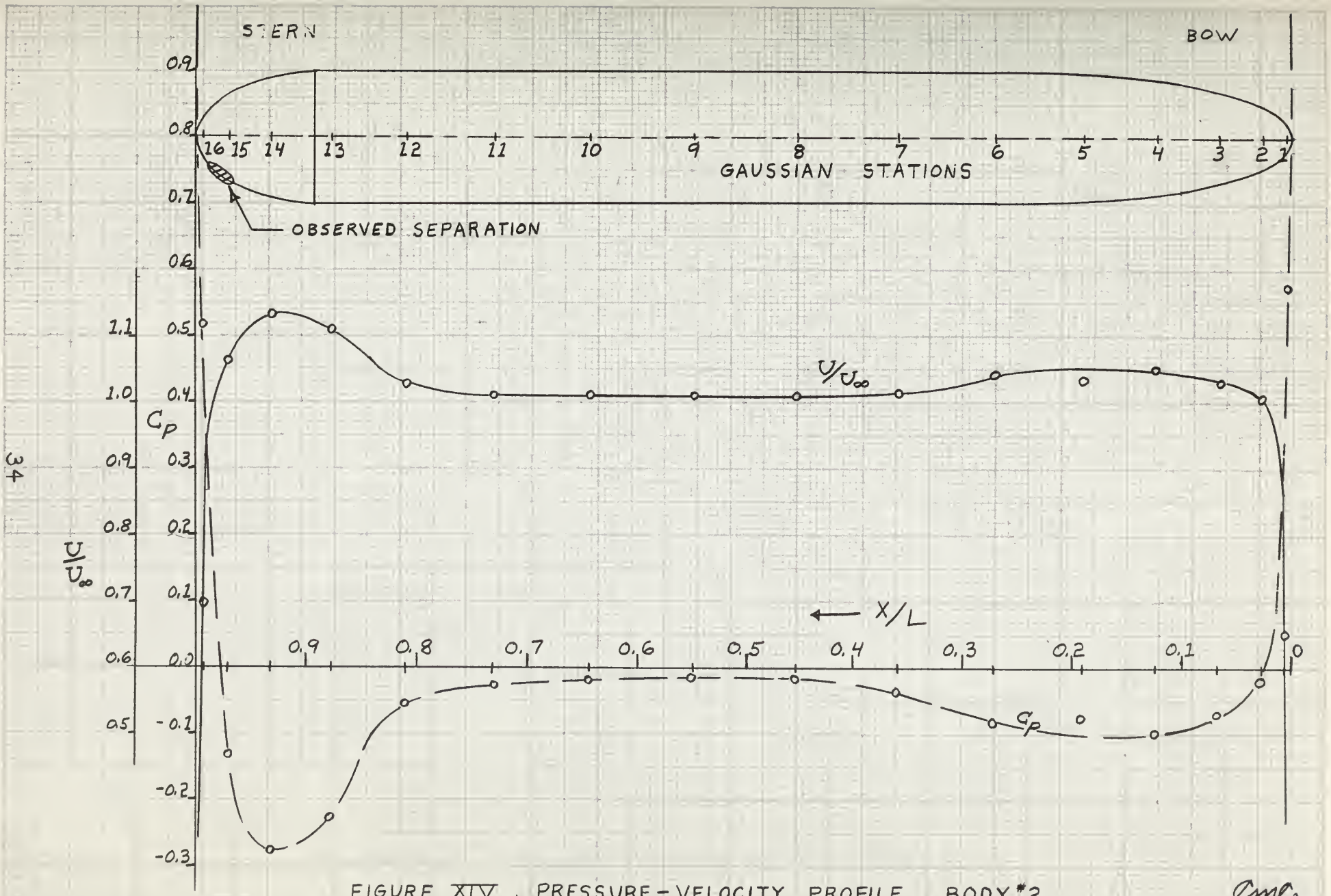

FIGURE XIV , PRESSURE-VELOCITY PROFILE , BODY #2

4/25/62

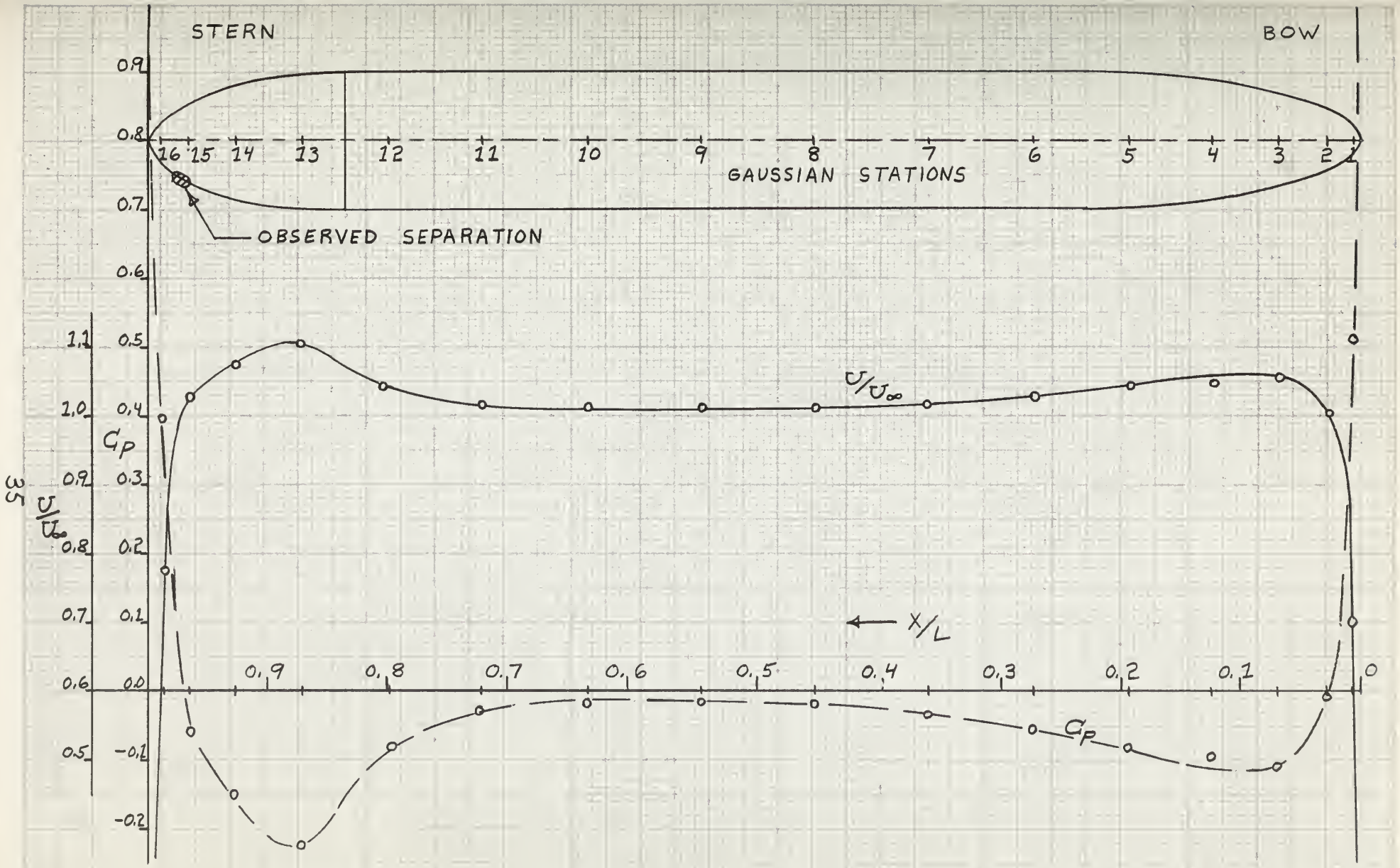

FIGURE XV , PRESSURE-VELOCITY PROFILE , BODY # 3

4/25/62

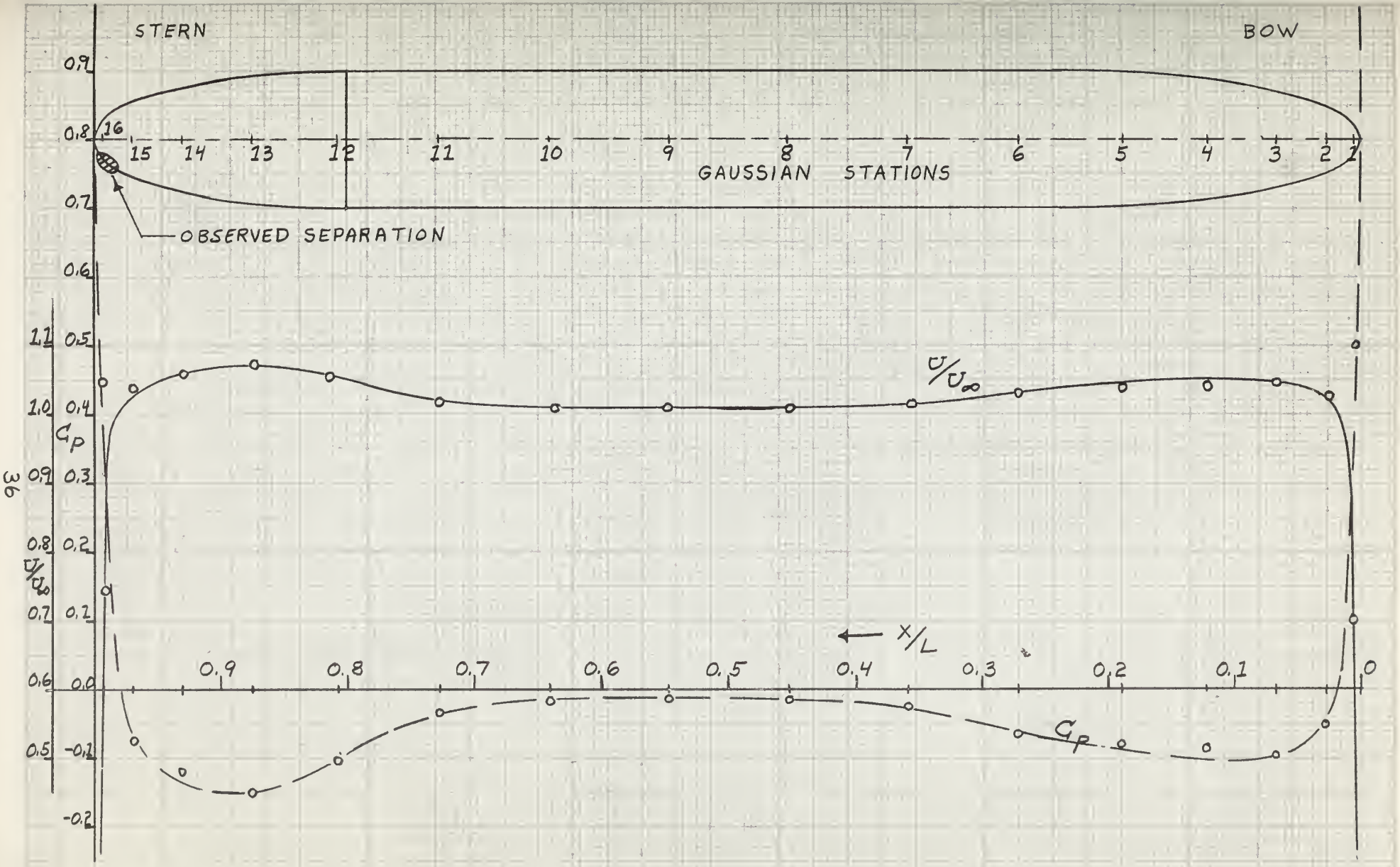

FIGURE XVI, PRESSURE-VELOCITY PROFILE, BODY # 4

Cmc
4/25/62

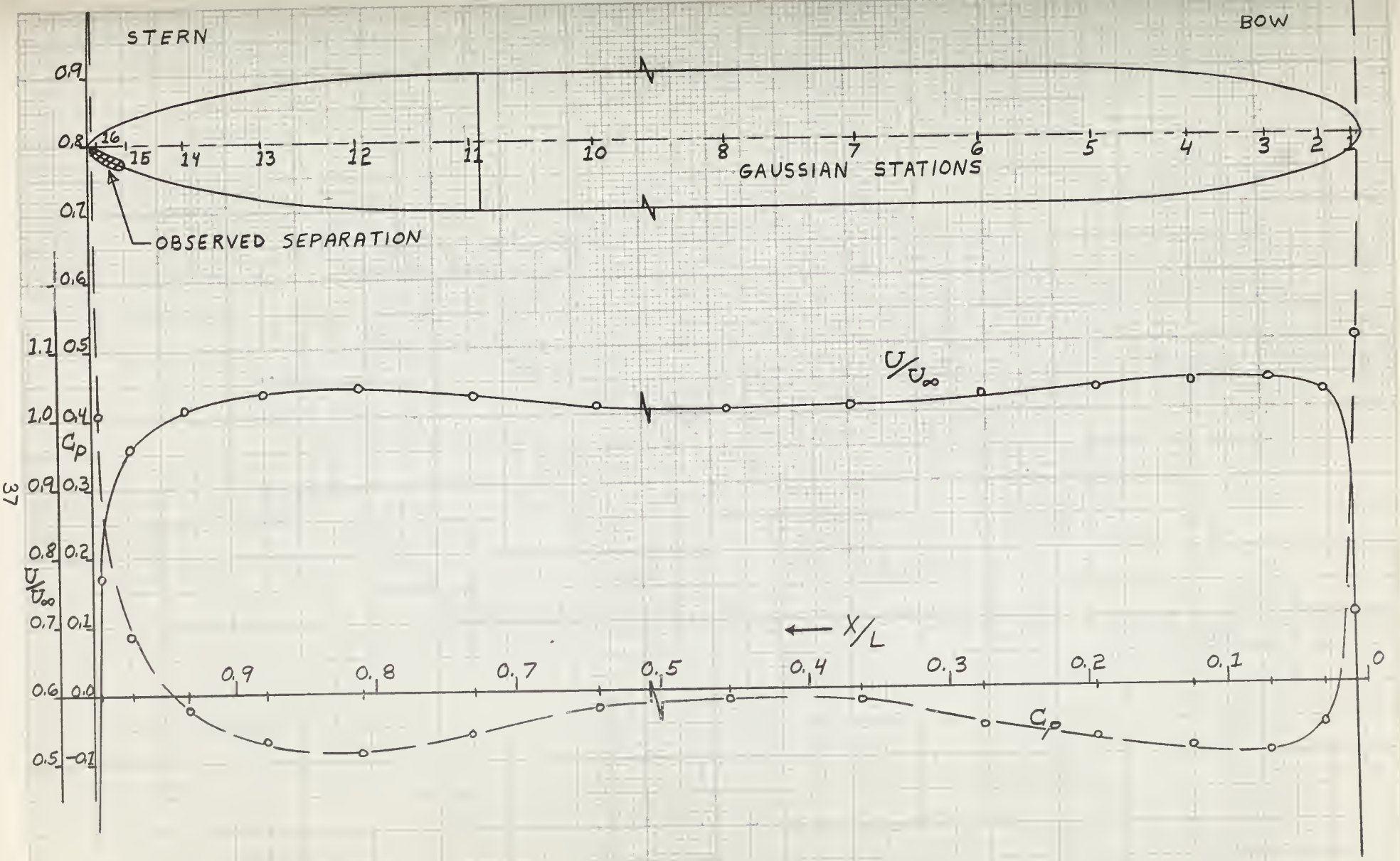

FIGURE XVII, PRESSURE-VELOCITY PROFILE, BODY #5

4/25/62

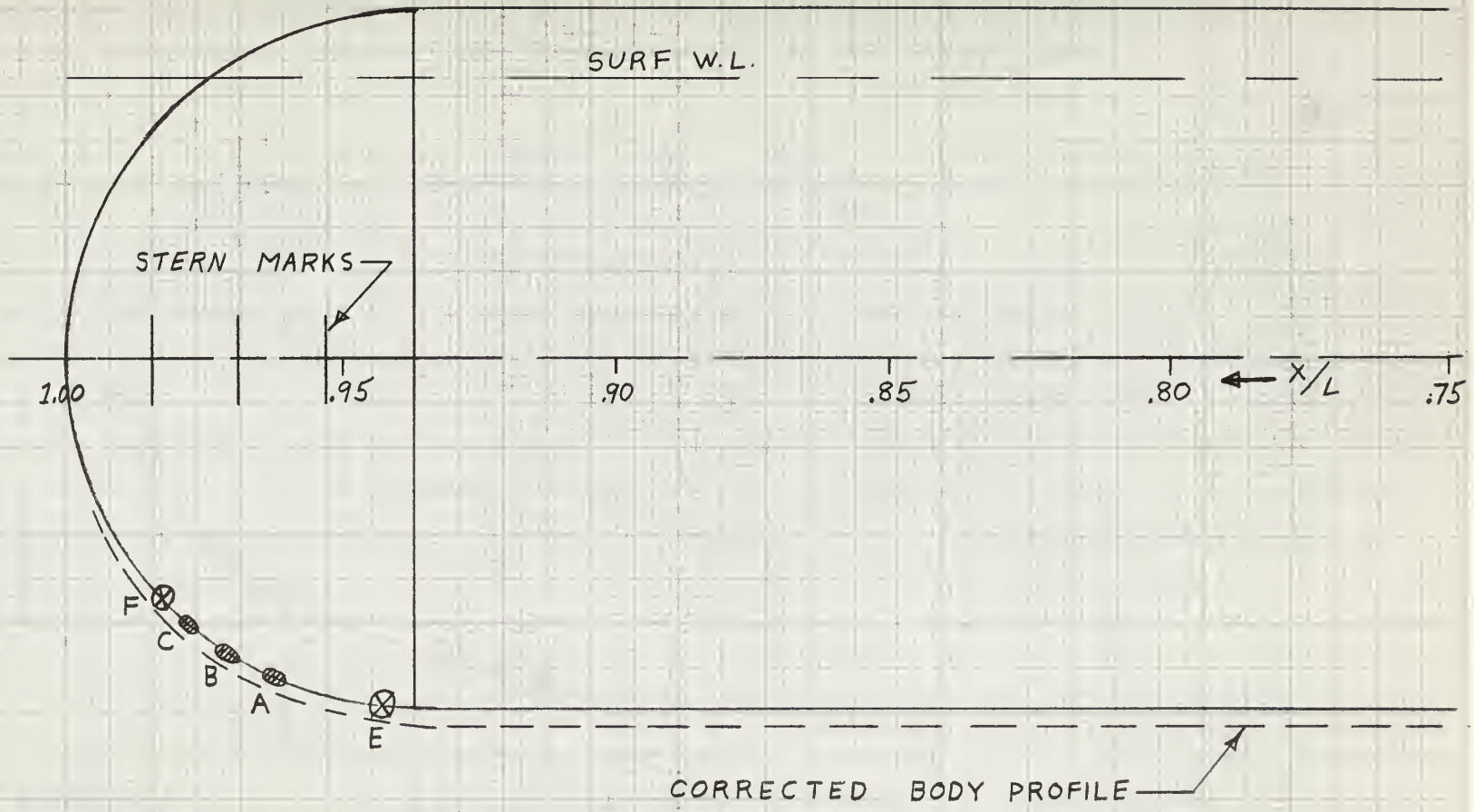

A - 24° EXPERIMENTAL
B - 32° "
C - 42° "
E - 6° BURI
F - 47° STRATFORD

FIGURE XVIII , SEPARATION POINTS , BODY #1

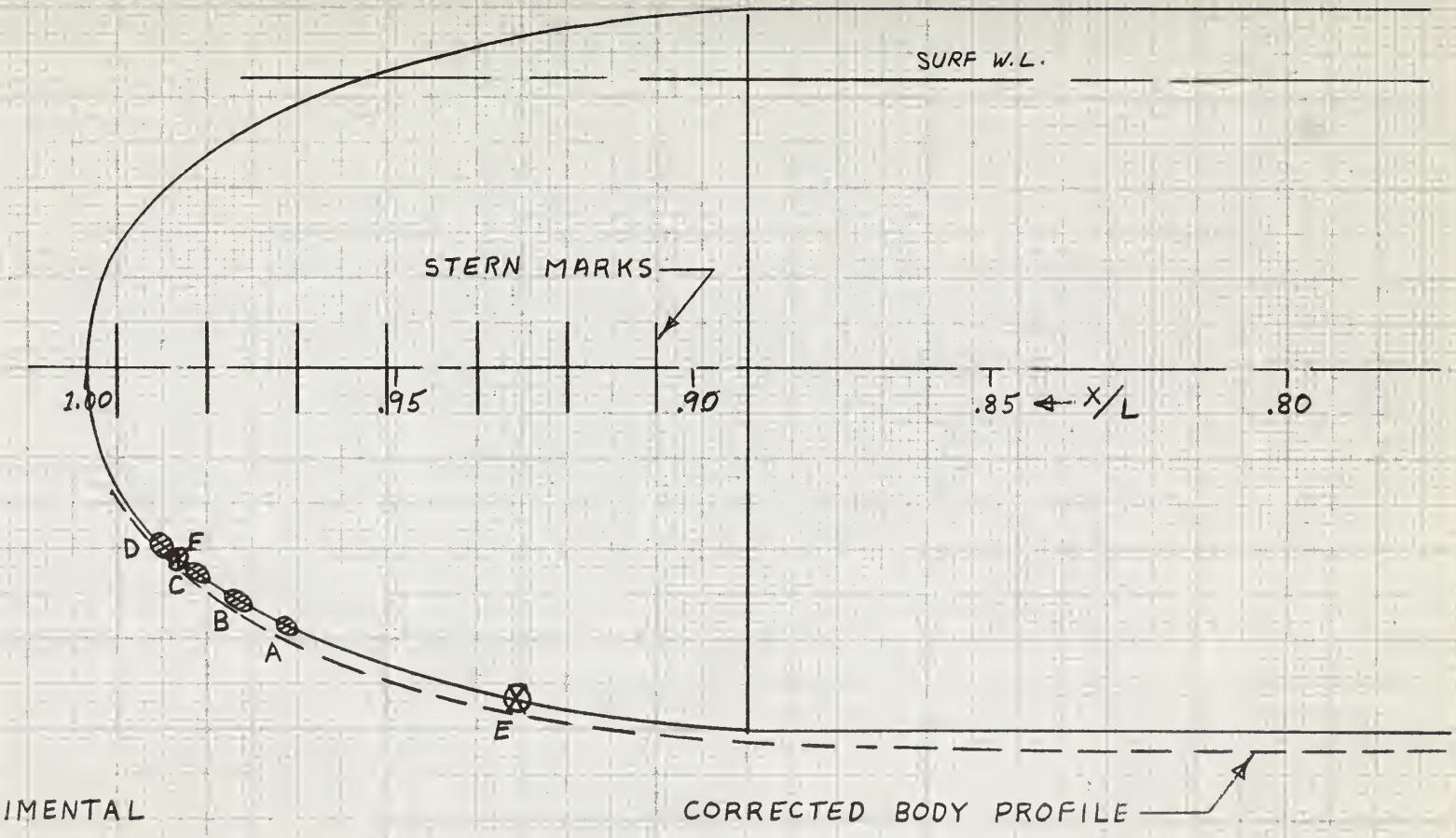

A - 25° EXPERIMENTAL
B - 30° "
C - 36° "
D - 42° "
E - 13° BURI
F - 38° STRATFORD

FIGURE XIX , SEPARATION POINTS , BODY #2

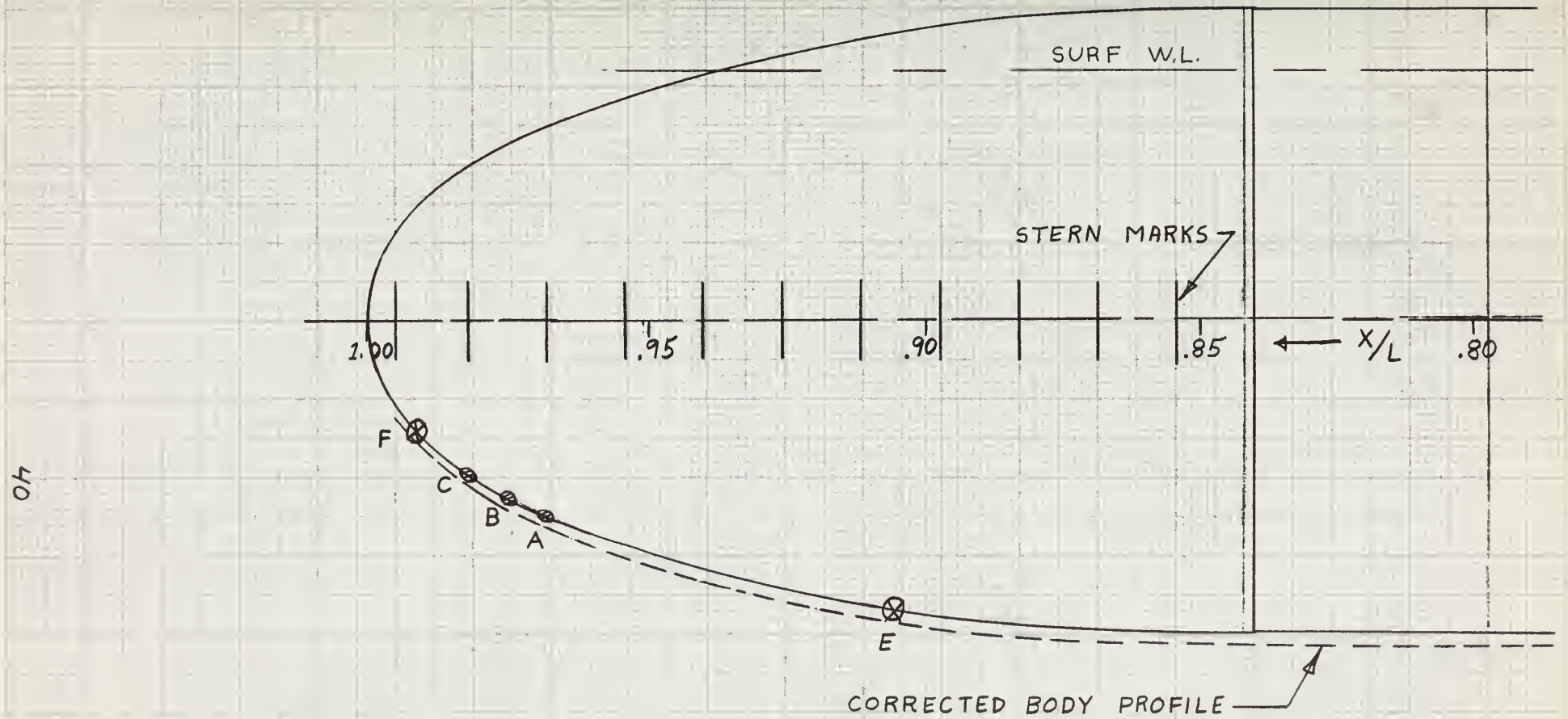

A - 23° EXPERIMENTAL
B - 28° "
C - 33° "
E - 10° BURI
F - 46° STRATFORD

FIGURE XX , SEPARATION POINTS , BODY #3

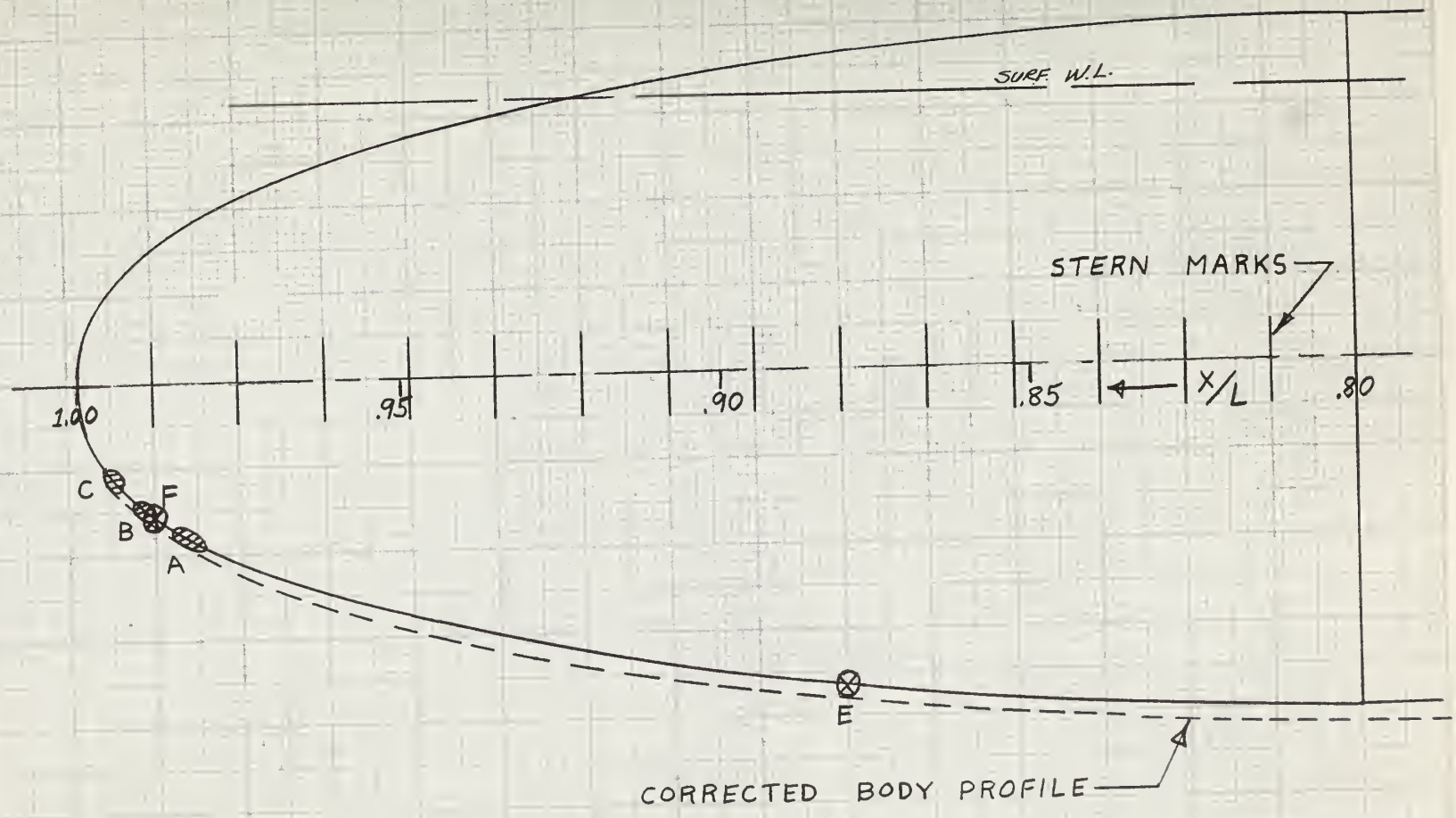

A - 28° EXPERIMENTAL
B - 38° "
C - 49° "
E - 6° BURI
F - 36° STRATFORD

FIGURE XXI , SEPARATION POINTS , BODY # 4

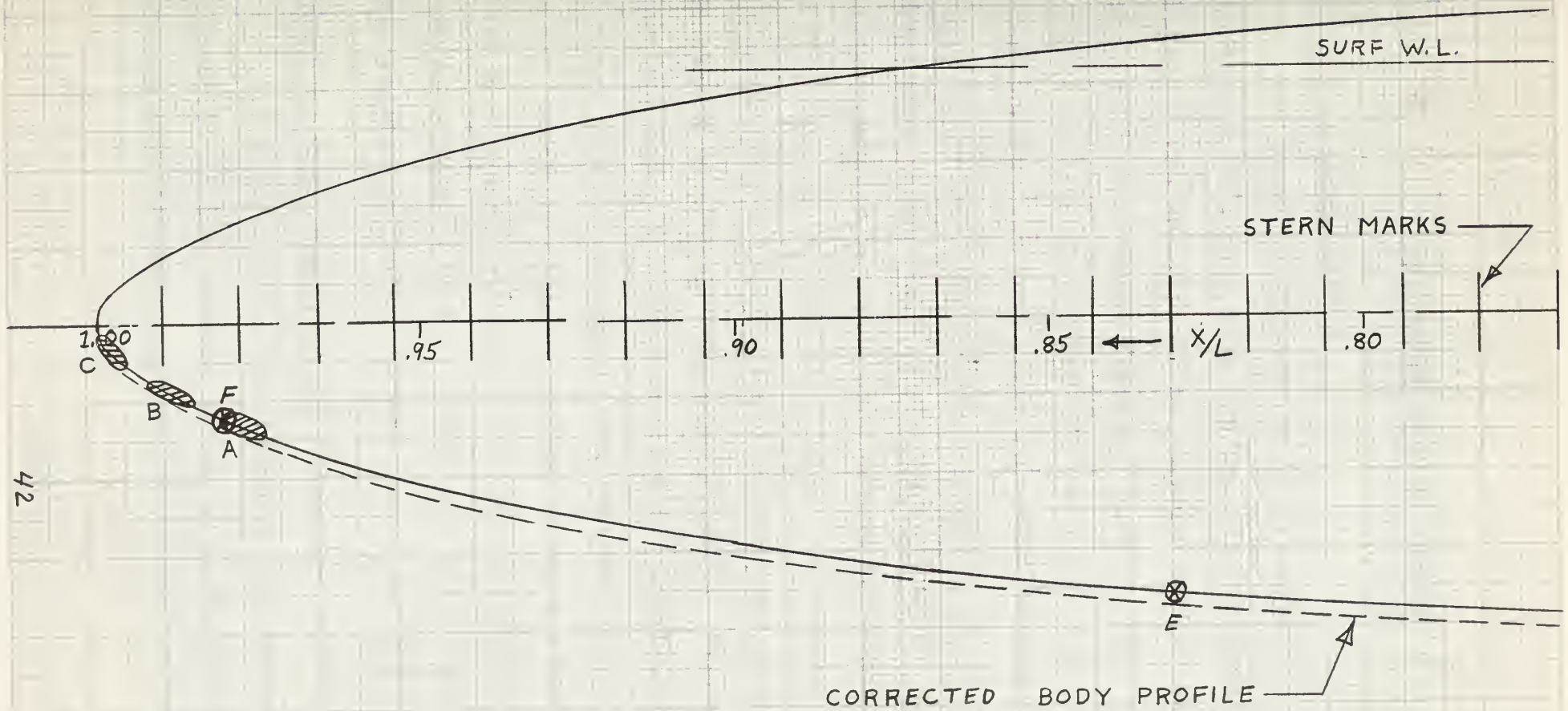

A - 23° EXPERIMENTAL
B - 30° "
C - 60° "
E - 5° BURI
F - 23° STRATFORD

FIGURE XXII , SEPARATION POINTS, BODY # 5

IV DISCUSSION OF RESULTS

Accuracy of Observations

The accuracy achieved in determining the location of the separation points from the dye-flow photographs was limited by the ability of the authors to pick off the point where the flow abruptly departed from the body surface and in their ability to interpolate between the ½ inch markings on the bodies. In some cases the point of separation was partially obscured by excessive amounts of dye while in other cases, especially at the higher speeds, a portion of the dye appeared to be carried beyond the separation point by flow outside the boundary layer. In the surface condition there was some evidence of dye being drawn up into the area aft of the body toward the free surface. The accuracy in observing the point of separation in turbulent flow can not be equal to that obtainable for laminar flow, but improvement in this accuracy could be gained by using a larger model and/or using a more sophisticated means of photographing the flow such as telephoto lens or underwater motion pictures to obtain greater definition of the flow about the body.

Effect of Body Closing Angle

In examining the positions of the observed points of separation on the various bodies as shown in Figures XVIII through XXII it was noted that the points occurred in groups

located at three or four positions on the bodies. Table I shows the details for these groupings. The center of each group was used as the measuring point of the body angles. The degree of accuracy obtained in measuring these angles is a function of the accuracy achieved in the initial location of the point of separation already discussed and the errors envolved in measuring the angle from the full scale drawings. The two factors result in a possible error of $\pm$ 3 degrees.

The initial group of separation points on all five bodies tested occurs at a body angle of between 23 and 28 degrees, averaging about 25 degrees. There is no apparent orderly correlation among the five bodies to account for this variation except that it is due to experimental error. This results in the conclusion that the initial point of separation occurs at approximately the same angle for all bodies regardless of the amount of streamlining. A critical angle of 25 degrees thus appears to be established for initiation of separation. The rate at which the body angle is changing does not appear to effect this critical angle because bodies 1 and 5 which have vastly different rates of change of body angle have nearly the same critical angle. A systematic check over a greater range of body shapes, speeds and depths of submergence is warranted to check this conclusion.

The maximum value of the angles in the region over which the separation points occurred varied from about 42 degrees

to 60 degrees showing that the observed point of separation did fluctuate. At these higher angles, however, the speeds were generally toward the high end of the speed range and the fluctuations may be caused by dye being carried aft by flow outside the boundary layer, especially on body 5 where the point of separation was most difficult to determine. Because of this possible effect these angles are not considered as significant as the initial separation angles. The above comment, notwithstanding, these higher angles do point up that under certain circumstances separation of flow may not occur until the critical angle has been exceeded by a considerable amount.

Evaluation of Separation Criteria

Buri's theoretical separation criterion equation (26), consistently predicts the separation point well forward of both the experimentally observed points and the point of separation established by Stratford's criterion, equation (21). For Buri's criterion the body angle values all fall between 5 and 13 degrees with no apparent consistency of variation, except that when body 1 is eliminated the angles decrease from body 2 to body 5, thus indicating that the separation point moves forward with increase in streamlining. This is inconsistent with the experimental results and the general concepts relating to separation which maintain that streamlining should decrease the extent of the separation zone,

not increase it. This criterion is very sensitive to slope of the curve of U/U_∞ versus X/L as plotted in Figure F-I, Appendix F, and relatively insensitive to model speed that enters through θ in (26). The criterion predicts separation to occur just as the value $d(U/U_\infty)/d(X/L)$ becomes negative. A slight error in plotting this curve or in using it to solve (26) could result in a larger error in the separation point; however, the magnitude of the possible error, ± 0.2 inch, is not sufficient to improve the agreement between Buri and the observed points.

On the other hand, Stratford's criterion gives much closer agreement with the experimentally observed points of separation, as it consistently predicts separation either within or slightly aft of the observed region of separation. The values of the body angles at the predicted separation points vary from 23 to 47 degrees. Again there is no apparent consistency of this variation. Depending on the shape of the curve of Cp versus X, as plotted in Figure F-II, Appendix F, this criterion is sensitive both to the value of Cp and the value of $d(C_p)/dx$ and also insensitive to model speed that enters through R_s and n in (21). Where the slope is steep the value of Cp is the controlling factor while for a shallower slope both Cp and $d(Cp)/dx$ control. The criterion essentially predicts separation to occur very shortly after Cp becomes positive. Again errors in plotting or interpreting Figure F-II

would not effect the predicted point of separation by more than ±0.1 inch.

It can be concluded that Buri's criterion did not give a satisfactory comparison to the observed point of separation while Stratford's agreed much better although it generally indicated that the body angle at separation was of a larger value than that observed. It is to be kept in mind, however, that these criteria were analyzed on the basis of the calculated profiles in Figures XIII through XVII which were derived for modified potential flow. It is therefore recommended that an experimental determination of velocity-pressure profiles be made on the bodies and that these be applied to the separation criteria before a final judgment is made.

Effect of Proximity of Free Surface

Table I yields no apparent consistent variation of the experimental points of separation on the various bodies with a change in operating depth.

Computer Program III calculates gage pressure or dynamic pressure plus hydrostatic pressure due to depth of submergence on each body. The variation in pressure at the keel is from about 19 lbs. per square foot at the surfaced condition to about 93 lbs. per square foot at the deep depth which should be sufficient to show the effect of change in depth on the observed location of the separation point if in fact such an effect on separation does exist. Both of the separation

criteria are completely independent of depth since it does not enter into any of the variables contained in equations (21) or (26). It is concluded from the experimental results that hydrostatic pressure over the range investigated has no recognized consistent effect on the location of the separation point.

It is recommended that further experimentation be conducted with larger variations in depth. Perhaps the use of a water tunnel or propeller tunnel would be better than a towing tank for this type of experiments since a large static pressure could be applied to the model in the test section. More typical ship shapes rather than body of revolution forms should be used in conducting dye-flow experiments in the air-water interface to show the effects of draft on separation over a given form.

Effect of Speed

Bodies I through 4 show values of the body angle at the separation point between 23 and 28 degrees for the low speed range, between 30 and 37 degrees for the medium speeds and 33 to 60 degrees for the high speeds. Because of the difficulty in locating the separation point for body 5, no relation between speed and separation point could be seen for that body. The results for bodies 1 through 4, however, show that the separation point appears to move aft on the body as speed increases. The reason for this effect could be due to the

fact that dye was being carried back along the body outside the boundary layer and misinterpretation of the photographs resulted. At the speeds used the Reynolds' Numbers were from 3.5 to 7 x 10^5. This is within the doubtful transition region between laminar and turbulent flow and the possibility exists that the lower speeds were at the laminar end of the transition, although an examination of the photos in Figure XII indicates a typical turbulent flow pattern. As speed increased the mere fully turbulent flow region was approached with the added increased effect of the trip wire with speed thus causing the point of separation to move aft on the body, as it does in a typical transition from laminar to turbulent flow. The two theoretical separation criteria are insensitive to changes in speed in the range investigated as has been previously discussed.

The recommendation here is obvious; the experiments must be conducted at higher speeds to further insure turbulent flow. In the present experiments the speeds obtainable were directly related to the ability to observe the dye flow, the dye being dissipated with increased speed and almost wholly indistinguishable beyond 1.75 knots. The speed limitation was due in part also to large carriage vibrations at higher speeds than those used. With a more refined method of turbulence stimulation and dye-flow observation techniques higher speeds could be attained leading to perhaps more con-

clusive and plausible results relating the effect of changing speed on the separation point than those herein achieved.

Corrected Body Profiles and Pressure-Velocity Profiles

Equivalent or corrected body profiles shown in Figures XVII through XXII are the results of Computer Program II. From the sample of these results given in Table G-I in Appendix G it can be noted that there is only a very slight variation in corrected profile on a given body with variation velocity. The corrected body profile radii decreased slightly with increase in speed. The variation is considered to be beyond the accuracy of the model construction and the full scale drawings so the corrected body profile was plotted the same for all velocities on a given body. In Figures XVIII through XXII the corrected body is plotted beyond the separation point however, this in fact does not exist since this profile is based upon modified potential flow theory which does not hold after separation occurs.

The pressure-velocity profiles for the bodies shown in Figures XIII through XVII are the results of Computer Program III. From the sample of these results given in Table G-II in Appendix G only a slight variation in Cp and U/U_{∞} occurs with variation of U_{∞} or model velocity. This is a result of the aforementioned slight variation in body profile with model velocity since the output of Program II, Y - NORM, is the input to Program III. Again this slight variation is considered

beyond the accuracy of the model drawings and certainly is not detectable when plotted at the scales used in Figure XIII through XVII. Thus the profiles appear the same for all velocities on a given body.

Since neither depth of submergence nor hydrostatic pressure enter into the calculations of the corrected body profile or pressure-velocity profiles none of the figures show a variation with depth.

In summary, the experimental results indicate that separation appears to begin at a critical angle of about 25 degrees irrespective of body streamlining. The correlation of separation with speed and depth is not clearly seen since the speed and depth range should be larger for more conclusive results. The results as pointed out in the introduction are qualitative in nature and are not be be construed as quantitative evidence. Such evidence must be provided in later works. The primary recommendation is that further studies be carried out at greater speeds with improvements in the technique of observing the separation point. Stratford's separation criterion, which is more rigorous than Buri's appears to give good agreement with the experimental observations, but it should be further evaluated by using experimentally determined pressure-velocity distributions.

V - CONCLUSIONS

The conclusions which were arrived at in IV are summarized as follows:

1. The observed position of separation was determined within an accuracy of $\pm$ 1/2 inch on the body and the body angle at this position was thereby determined to $\pm$ 3^{o}.

2. Initial separation occurs at body angles of between 23^{o} and 28^{o} regardless of the amount of body streamlining.

3. Buri's criterion for separation consistently predicts separation well forward of the observed separation point and thus does not compare favorably with the observed results.

4. Stratford's criterion evaluated from the calculated pressure-velocity distributions over the bodies gives reasonably close agreement with the location of the observed separation point.

5. Results of analyzing the separation position location show that it moves aft with increase in speed but this may be due to the fact that at the speeds investigated the Reynolds numbers were in the transition region between laminar and turbulent flow.

6. The theoretical criteria evaluated are both insensitive to body speed changes and are independent of the depth of submergence of the body.

7. The observed separation point does not move in a consistent manner on the body with a variation in depth of submergence of the body.

8. The corrections applied to the body surface to account for boundary layer effects showed little change with change in body speed for a given body.

9. The pressure-velocity profiles over the bodies calculated from modified potential flow showed little change with change in body speed for a given body.

VI - RECOMMENDATIONS

The recommendations made in IV are summarized as follows:

1. Further experimentation should employ a larger model if possible and an improved means of observing the flow about the separation point.

2. A greater range of speeds and depths should be investigated in future work to increase the reliability of the data obtained. Higher speeds consistent with the ability to observe the dye-flow are necessary to insure that flow is definitely in the turbulent region.

3. If higher speeds can not be attained improvement should be made in the method of inducing turbulence through stimulation.

4. If dye studies are continued a minimum of dye should be used to prevent dye outside the boundary layer from obscuring the observations.

5. Pressure measurements should be made in and ahead of the separation zone to experimentally determine the pressure-velocity distribution over the bodies and also serve as another method of locating the separation point. This could be compared with the results of this work and used to re-evaluate the separation criteria on the basis of

the actual pressure-velocity profiles rather than on calculated profiles. This appears to be the next logical step as the initial determination of the separation zone has been made in this work.

6. Recommendations relating to drag force measurements are included in Appendix E.

VII APPENDIX

APPENDIX A
OFFSETS AND OTHER CHARACTERISTICS FOR MODEL AND STERN SECTIONS

TABLE A-I - OFFSETS

Body: Station Spacing: Station 0 at: Station:	Nose Section 0.50" Nose Radius (Inches)	Stern 1 0.50" Tail Radius	Stern 2 0.50" Tail Radius	Stern 3 0.50" Tail Radius	Stern 4 0.50" Tail Radius	Stern 5 0.50" Tail Radius
0	0.00		0.00	0.00	0.00	0.00
0.5	0.43		0.80	0.65	0.63	0.32
1	0.68		1.05	0.87	0.85	0.47
1.5	0.83		1.23	1.03	0.98	0.57
2	0.94		1.37	1.16	1.09	0.69
3	1.12		1.58	1.36	1.27	0.87
4	1.27		1.72	1.52	1.41	1.00
5	1.37		1.84	1.66	1.53	1.12
6	1.47		1.93	1.77	1.63	1.23
7	1.54		1.98	1.84	1.72	1.33
7.26	--		2.00	--	--	--
8	1.62			1.91	1.78	1.42
9	1.67			1.95	1.84	1.50
10	1.72			1.98	1.89	1.57
11	1.76			1.99	1.93	1.63
11.30	--			2.00	--	--
12	1.80				1.96	1.69
13	1.83				1.98	1.74
14	1.87				1.99	1.79
14.78	--				2.00	--
15	1.90					1.83
16	1.93					1.87
17	1.95					1.90
18	1.96					1.92
19	1.97					1.94
20	1.99					1.96
21	2.00					1.98
22	--					1.99
22.78	--					2.00

HEMISPHERE OF RADIUS = 2.00 INCHES

TABLE A-II- OTHER CHARACTERISTICS

	Nose/Tail Radius (inches)	Length (inches)	Wetted Surface Depths 1 and 2 (sq.ft.)	Wetted Surface Depth 3 (sq.ft.)
Nose	0.43	10.5	0.726	0.640
Cylindrical Section	--	19.0	1.653	1.311
Stern 1	2.00	2.00	0.175	0.158
Stern 2	1.47	3.63	0.245	0.219
Stern 3	0.98	5.65	0.387	0.340
Stern 4	0.99	7.39	0.513	0.454
Stern 5	0.33	11.39	0.741	0.664
Body 1	--	31.50	2.554	2.109
Body 2	--	33.13	2.624	2.170
Body 3	--	35.15	2.766	2.291
Body 4	--	36.89	2.892	2.405
Body 5	--	40.89	3.120	2.615

Body means total of nose, cylindrical section, and stern shape.

Wetted surfaces submerged (depths 1 and 2) were calculated using ten-ordinate Simpson's rule with half-stations on body perimeters.

Spacings of 1 inch were used on nose and stern 5, 3/4 inch on stern 4, 1/2 inch on sterns 2 and 3. Stern 1 was calculated directly since it was a hemisphere.

Surfaced wetted surfaces (Depth 3) were calculated by computing non-wetted surface using trapezoidal rule on non-wetted arc lengths and subtracting from submerged wetted surface values.

These calculations are not shown in this report.

TABLE A-III

GAUSSIAN STATION, RADIUS, AND BODY ANGLE

Gaussian Station	$\frac{X}{L}$	Body 1			Body 2			Body 3		
		X	Radius	Angle	X	Radius	Angle	X	Radius	Angle
-.990	.005	0.17	0.37	49.5	0.18	0.37	49.4	0.19	0.40	47.3
-.944	.028	0.87	0.88	26.0	0.92	0.91	25.0	0.97	0.94	23.9
-.866	.067	2.12	1.30	14.2	2.23	1.31	12.7	2.36	1.37	11.7
-.756	.122	3.85	1.60	7.5	4.05	1.63	7.1	4.30	1.67	6.3
-.618	.191	6.02	1.81	4.5	6.33	1.84	4.4	6.72	1.87	3.6
-.458	.271	8.54	1.96	2.6	8.98	1.98	1.8	9.52	1.97	1.5
-.282	.359	11.31	2.00	0.0	11.90	2.00	0.0	12.62	2.00	0.0
-.096	.452	14.25	2.00	0.0	14.99	2.00	0.0	15.90	2.00	0.0
+.096	.548	17.25	2.00	0.0	18.14	2.00	0.0	19.24	2.00	0.0
+.282	.641	20.19	2.00	0.0	21.23	2.00	0.0	22.52	2.00	0.0
+.458	.729	22.96	2.00	0.0	24.15	2.00	0.0	25.62	2.00	0.0
+.618	.809	25.48	2.00	0.0	26.80	2.00	0.0	28.43	2.00	0.0
+.756	.878	27.65	2.00	0.0	29.08	2.00	0.0	30.85	1.94	5.1
+.866	.933	29.38	2.00	0.0	30.90	1.78	13.1	32.79	1.62	15.5
+.944	.972	30.63	1.63	35.0	32.21	1.33	27.8	34.18	1.15	24.5
+.990	.995	31.33	0.78	67.2	32.95	0.69	59.6	34.96	0.57	51.5

Gaussian Station	$\frac{X}{L}$	Body 4			Body 5		
		X	Radius	Angle	X	Radius	Angle
-.990	.005	0.20	0.41	47.1	0.21	0.42	46.5
-.944	.028	1.02	0.97	22.7	1.13	1.00	21.6
-.866	.067	2.48	1.38	11.5	2.75	1.42	10.0
-.756	.122	4.51	1.67	5.7	5.00	1.72	5.1
-.618	.191	7.05	1.88	3.4	7.81	1.91	2.7
-.458	.271	10.00	1.99	1.0	11.08	2.00	0.0
-.282	.359	13.25	2.00	0.0	14.69	2.00	0.0
-.096	.452	16.69	2.00	0.0	18.50	2.00	0.0
+.096	.548	20.20	2.00	0.0	22.39	2.00	0.0
+.282	.641	23.64	2.00	0.0	26.20	2.00	0.0
+.458	.729	26.89	2.00	0.0	29.81	1.98	1.0
+.618	.809	29.84	1.99	1.0	33.07	1.85	4.1
+.756	.878	32.38	1.84	6.2	35.89	1.57	8.3
+.866	.933	34.41	1.52	12.0	38.14	1.18	12.9
+.944	.972	35.87	1.10	22.0	39.76	0.73	20.4
+.990	.995	36.69	0.55	53.0	40.67	0.28	36.4

Note:

X is inches from nose of body.
Radius is in inches.
Angle is in degrees.

APPENDIX B - DESCRIPTION OF TOWING TANK AND INSTRUMENTATION

An early description of the Ship Model Towing Tank, prior to the installation of the towing carriage, is given in a paper entitled "The Ship Model Towing Tank at M.I.T.," Society of Naval Architects and Marine Engineers, 1953. This paper does, however, give an up to date description of the tank dimensions and the speed measuring and counting equipment. Since the towing carriage was installed late in 1961, a brief description will be included here.

The carriage is constructed of aluminum and rides on two hollow cylindrical stainless steel rails, one overhead and one mounted on the tank's side wall. The overhead rail is simply for support and guidance of the carriage which rides it on six fibreglass wheels, two above and one below the rail at either end of the carriage frame. The carriage is also supported by the side rail with three wheels riding on the after end and a soft rubber drive wheel connected via a coupling to an electric motor on the forward end. The electric drive motor is controlled by the console at one end of the tank via cables attached to pulleys which slide along a smaller rail mounted on the tank wall above the side rail. The control cables are free riding and consequently as the carriage moves from one end of the tank to the other the speed decreases as more cable length is either drawn out from one end or piled up. A differential pulley system was installed which helped in alleviating this situation to some degree.

The carriage speed can be controlled either manually by setting a dial on the console or automatically at a set speed or to position the carriage over a self propelled model. The automatic control was inoperative during the period of the experiments included in this thesis, and speed was controlled manually. The speed measuring apparatus includes a type 500 Hewlett Packard frequency meter and a type 521 Hewlett Packard counter described in greater detail in the foremention reference.

Figure B-I shows a schematic drawing of the model dye system which is self-explanatory and figure B-II shows the details of the drag measuring towing dynamometer.

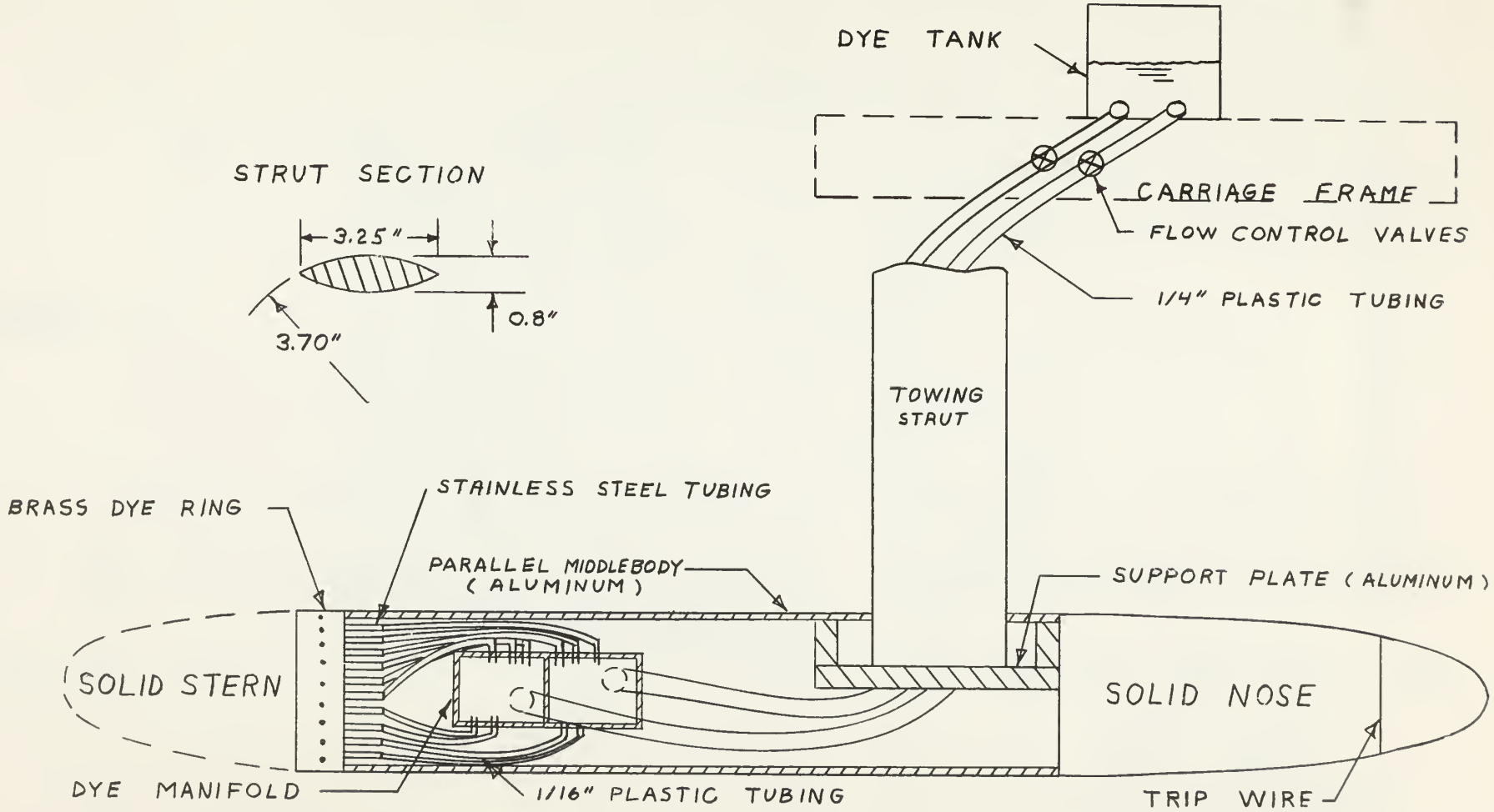

FIGURE B-I, MODEL DYE SYSTEM

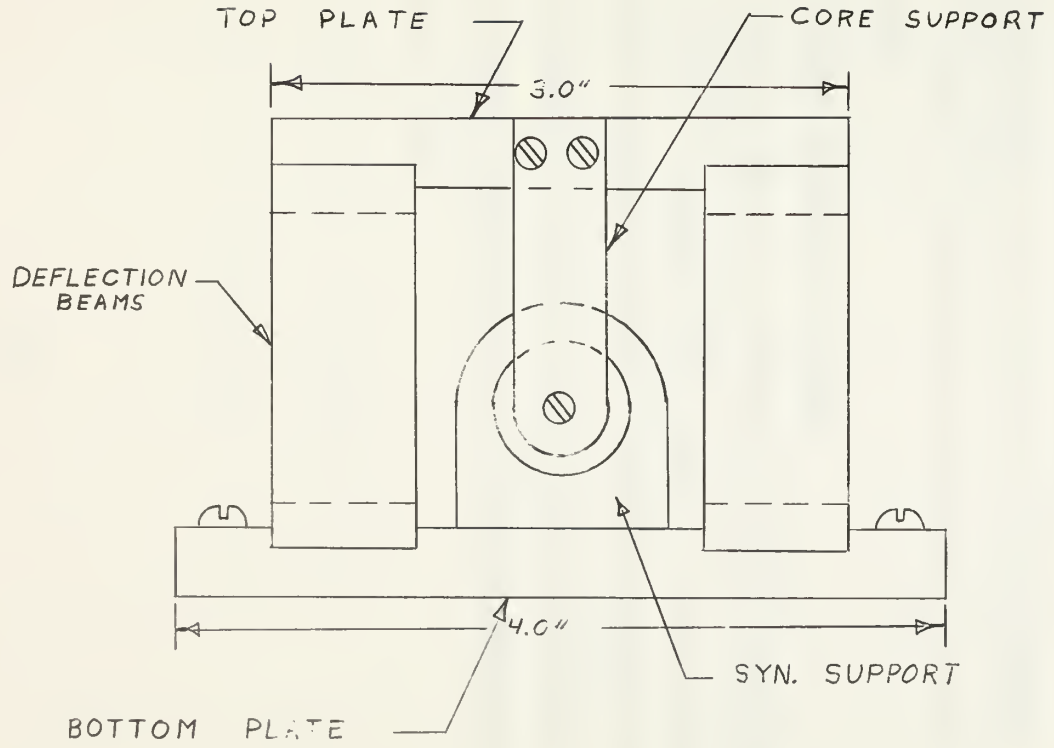

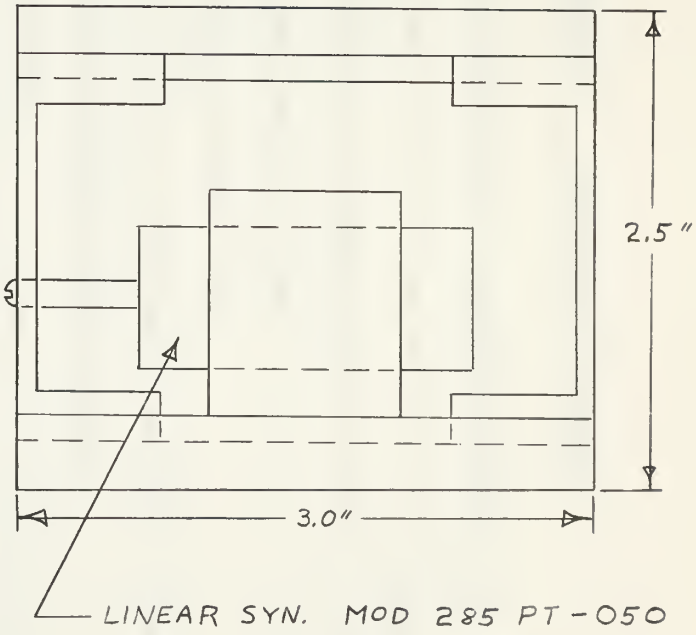

DWG NO. TD-2
MIT SMTT
TOWING DYNAMOMETER
SCALE 1"=1" 1/20/62
M.P.

FIGURE B-II DYNAMOMETER DETAILS

APPENDIX C - COMPUTER PROGRAMS

The IBM 7090 electronic computer located at the M.I.T. Computation Center was utilized as an aid in reducing drag data and in computing the theoretical portions of the thesis.

Three programs were written:

Program I - Reduction of drag data.

Program II- Calculation of turbulent boundary layer characteristics on the bodies tested.

Program III- Calculation of the pressure velocity distribution on the bodies tested.

These programs were written in 7090 FORTRAN. On the next several pages the following are given for each of the three programs:

1. FORTRAN program listing.
2. A list of program symbols and their meanings.
3. A logical sequence flow chart of the program.

Both FORTRAN and compiled binary machine language card decks and listings are available for these programs in the Department of Naval Architecture and Marine Engineering computer program files.

PROGRAM I - LISTING OF SYMBOLS

SYMBOL	MEANING	UNITS
RO	Mass density of tank water	$slug/ft.^3$
VIS	Kinematic viscosity of tank water	$ft.^2/sec.$
SLEN(N)	Body length	ft.
WSUR(N,M)	Wetted surface of body at particular depth	$ft.^2$
DT(L,M,N)	Measured drag	lbs.
V(L,M,N)	Model velocity	kts.
N	Body index	
M	Depth index	
L	Speed index	
SL	Lenth of strut submerged	inches
DSTR	Strut drag	lb.
DTC	Corrected body drag	lb.
SLR	Speed - length ratio($V/\sqrt{L}$)	$\frac{kt.}{\sqrt{ft.}}$
RM	Reynolds number on SLEN (N)	
A	$1/2\ \rho\ S\ V^2$	lb.
CT	Total drag coefficient	
CFSG	Friction drag coefficient using Shultz-Grunow formulation	
CFS	Friction drag coefficient using Schoenherr formulation	
CR	Residual drag coefficient	

LOGICAL SEQUENCE FOR PROGRAM 1

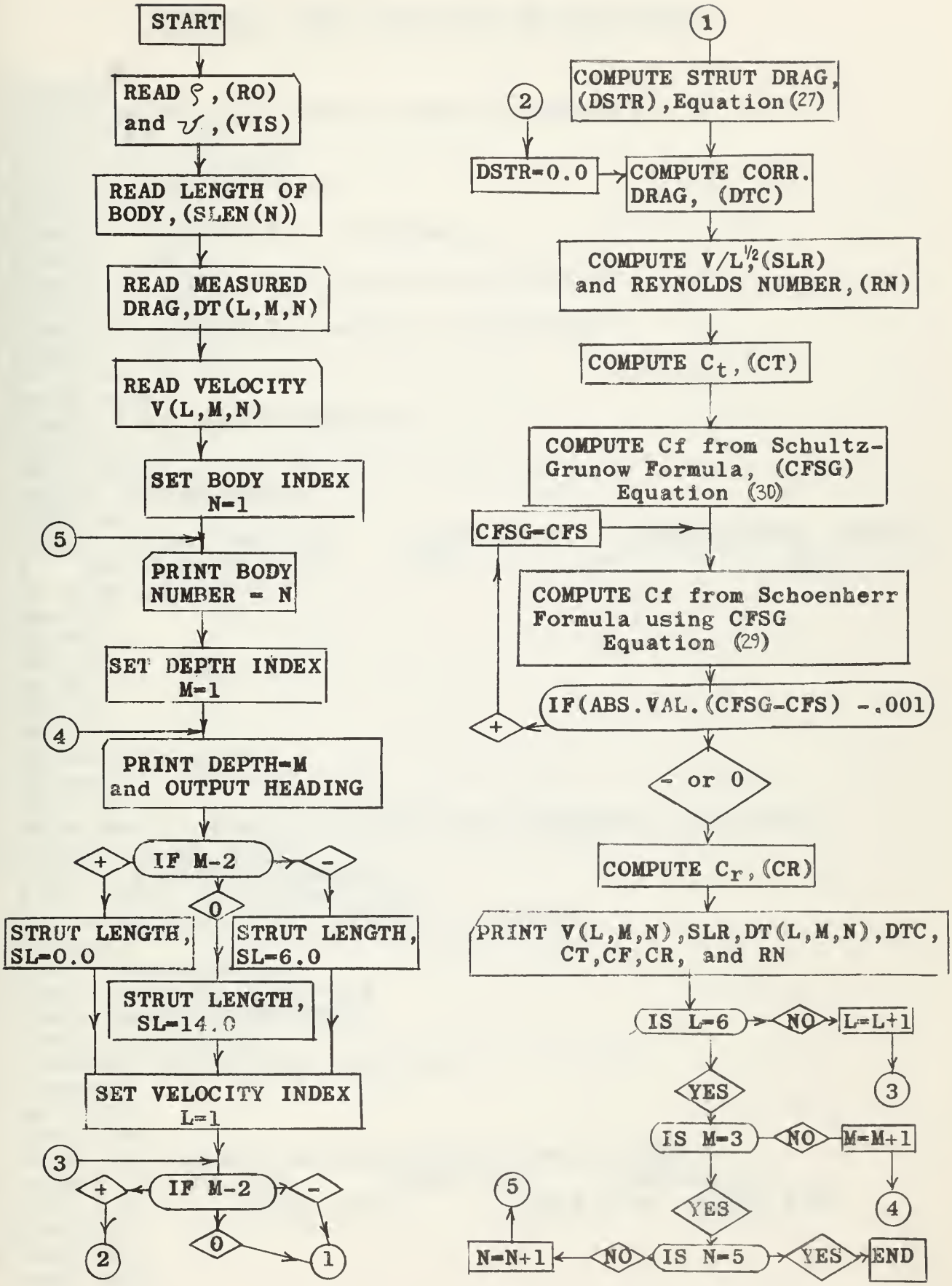

PROGRAM I FOR CALCULATION OF CR ON BODY

```
   FORTRAN
   DIMENSION DT(6,3,5),V(6,3,5),SLEN(5),WSUR(5,3)
   READ 24,RO, VIS
24 FORMAT (F5.3, E1Ø.4)
   READ 25,(SLEN(N),N=1,5)
25 FORMAT (5F4.2)
   READ 26, ((WSUR(N,M), N=1,5),M=1,3)
26 FORMAT (14F5.3)
   READ 27, (((DT(L,M,N), L=1,6) M=1,3),N=1,5)
27 FORMAT (18F4.2)
   READ 28, (((V(L,M,N), L=1,6), M=1,3),N=1,5)
28 FORMAT (18F4.2)
   DD 5Ø N=1,5
   PRINT 32,N
32 FORMAT (14H1 BODY NUMBER=I1)
   DD 5Ø M=1,3
   PRINT 33,M
33 FORMAT (8HØ DEPTH=I1)
   PRINT 34
34 FORMAT (111HØ  VEL.(KT)      REYNOLDS NO.     SPEED/LENGTH  TOT.DRA
 1 G    TOT.DRAG(CORR)          CT            CF              CR/)
   IF (M-2) 1Ø,11,12
1Ø SL=14.Ø
   GO TO 14
11 SL=6.Ø
   GO TO 14
12 SL=Ø.Ø
14 DO5Ø L=1,6
   IF (M-2) 61,61,6Ø
6Ø DSTR=Ø.Ø
   GO To 62
61 DSTR=(RO*((1.689*V(L,M,N))**2.Ø)*((Ø.Ø64*SL)+1.17))/288.Ø
62 DTC=DT(L,M,N)- DSTR
   SLR=V(L,M,N)/SQRTF(SLEN(N))
   RN=1.689*V(L,M,N)*SLEN(N)/VIS
   A=Ø.5*RO*WSUR(N,M)*(1.689*V(L,M,N))**2.Ø
   CT=DTC/A
   X1=Ø.434294*LOGF(RN)
   CFSG=Ø.Ø725/(X1-2.Ø)**2.Ø
13 X2=Ø.434294*LOGF(RN*CFSG)
   CFS=Ø.Ø585/x2**2.Ø
   IF(ABSF(CFSG-(Ø.ØØ1E-Ø3))7,7,15
15 CFSG=CFS
   GO TO 13
 7 CR=CT-CFS
   PRINT 35, V(L,M,N),RN,SLR,DT(L,M,N),DTC,CT,CFS,CR
35 FORMAT (3H  F4.2,7H       1PE1Ø.3,9H       ØPF5.2,1CH
  1ØPF5.3,8H       ØPF5.3,1ØH          1PE1Ø.3,4H   1PE1Ø.3,5H
  21PE1Ø.3)
5Ø CONTINUE
   CALL EXIT
   END
```

PROGRAM II - LISTING OF SYMBOLS

Symbol	Meaning	Units
P	Reciprocal of power in velocity profile	-
VIS	Kinematic viscosity of tank water	$ft.^2/sec.$
SLEN(N)	Body length	ft.
V(L,M,N)	Model velocity	kts.
X(I,N)	Distance from body nose	inches
R(I,N)	Radius of body at X(I,N)	inches
AL(I,N)	Cosine of angle between body surface and body axis at X(I,N)	-
N	Body index	-
M	Depth index	-
L	Speed index	-
I	Location on body index	-
RN	Reynolds number on X	-
PBLT	Boundary layer thickness on flat plate (δ pl)	inches
PDT	Displacement thickness on flat plate (δ^* pl)	inches
BLTO	Estimate of boundary layer thickness on body	inches
BLT	Boundary layer thickness on body (δ)	inches
A	Ratio of boundary layer thickness to model radius	--
DLNP	$\triangle$ n pl	--
DLTNP	$\triangle 2n$ pl	--
DT	Displacement thickness on body (δ^*)	inches

PROGRAM II (CONT'D)

Symbol	Meaning	Units
OMNP	$\Omega_{n_{pl}}$	--
OMTNP	$\Omega_{2n_{pl}}$	--
BMT	Momentum thickness on body (θ)	inches
RC	Body radius corrected to account for displacement thickness	inches
Y	Normalized radius	

LOGICAL SEQUENCE FOR PROGRAM II

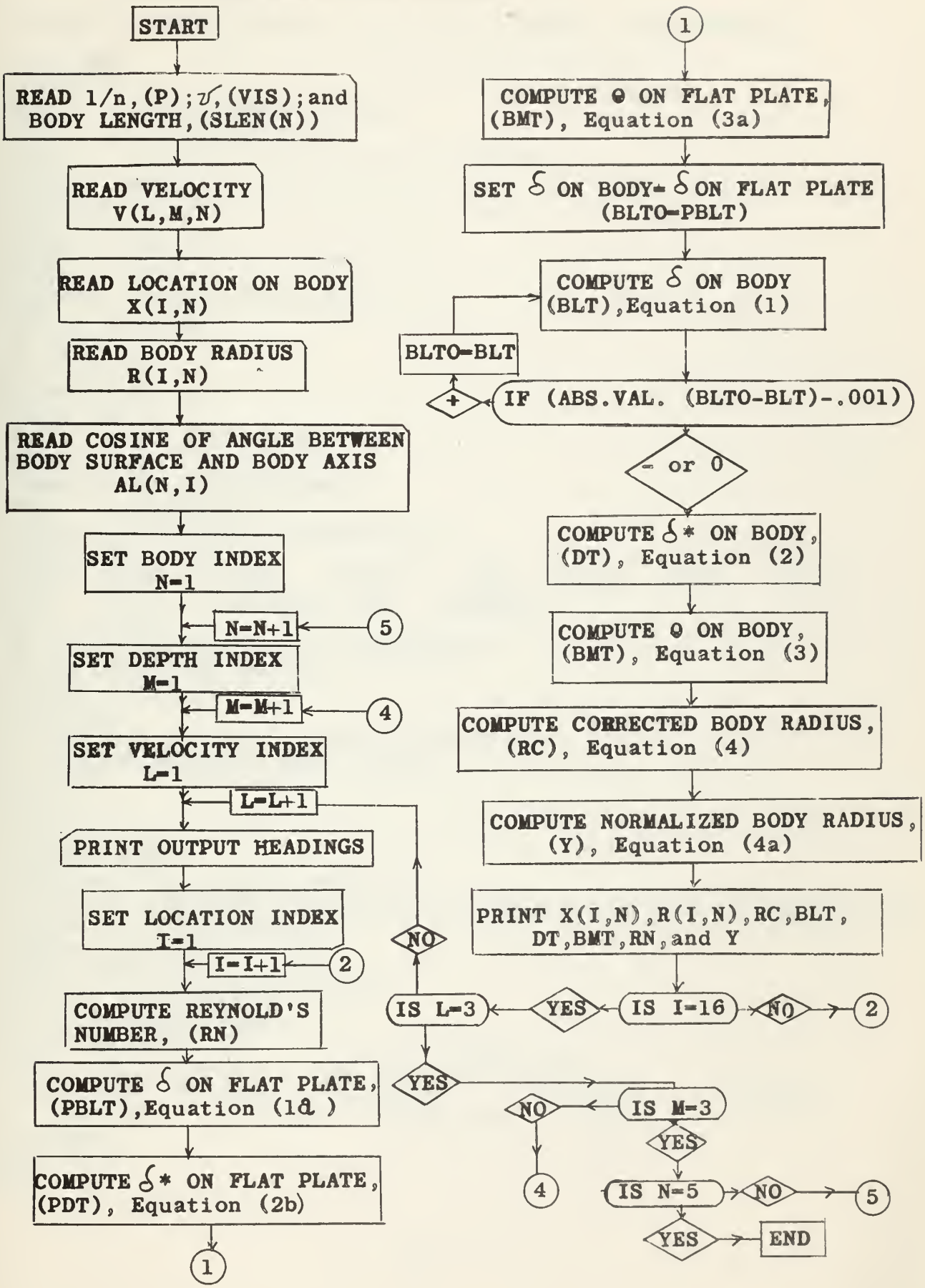

PROGRAM II, CALCULATION OF BODY DISPLACEMENT THICKNESS,ETC.

```
    FORTRAN
    DIMENSION V(3,3,5),X(16,5),R(16,5),SLEN(5),AL(16,5)
    READ 21,P,VIS,(SLEN(N),N=1,5)
 21 FORMAT (F3.1,E1Ø.4,5F4.2)
    READ 22,(((V(L,M,N),L=1,3),M=1,3),N=1,5)
 22 FORMAT (18F4.2)
    READ 23,((X(I,N),I=1,16),N=1,5)
 23 FORMAT(14F5.2)
    READ 24,((R(I,N),I=1,16),N=1,5)
 24 FORMAT (16F4.2)
    READ 25,((AL(I,N),I=1,16),N=1,5)
 25 FORMAT (14F5.3)
    DO 5Ø N=1,5
    DO 5Ø M=1,3
    DO 5Ø L=1,3
    PRINT 1ØØ,N
1ØØ FORMAT (14H2 BODY NUMBER=I1)
    PRINT 11Ø,M
11Ø FORMAT (13HØ BODY DEPTH=I1)
    PRINT 1Ø1,V(L,M,N)
1Ø1 FORMAT (16HØ VELOCITY(KTS)=F4.2)
    PRINT 1Ø2
1Ø2 FORMAT (95HØ  X(INCH)   RADIUS   CORR. RADIUS   DELTA   DELTA
   1STAR   THETA    REYNOLDS  NO.  Y-NORM/)
    DO 5Ø I=1,16
    RN=1.689*V(L,M,N)*X(I,N)/(VIS*12.Ø)
    PBLT=Ø.38*X(I,N)/RN**Ø.2
    PDT=PBLT/(1.Ø+P)
    BLTO=PBLT
 12 BLT=PBLT/(1.Ø+(BLTO/(3.Ø*R(I,N))))**Ø.8
    IF (ABSF(BLTO-BLT)-.ØØ1) 7,7,1Ø
 1Ø BLTO=BLT
    GO TO 12
  7 A=BLT/R(I,N)
    DLNP=PDT/PBLT
    DLTNP=DLNP*(P+1.Ø)/(2.Ø*P+1.Ø)
    DT=PDT*(1.Ø+A-SQRTF(1.Ø+2.Ø*A*(1.Ø-DLNP)+(A**2.Ø)*(1.Ø-DLTNP)))/(A
   1 *DLNP*(1.Ø+A/3.Ø)**Ø.8)
    OMNP=P/((P+1.Ø)*(P+2.Ø))
    OMTNP=OMNP*(P+2.Ø)/2.Ø*P+1.Ø)
    BMT=BLT*(OMNP+A*OMTNP/2.Ø)
    RC=R(I,N)+AL(I,N)*DT
    Y=RC/(SLEN(N)*6.Ø)
    PRINT 1Ø3,X(I,N),R(I,N),RC,BLT,DT,BMT,RN,Y
1Ø3 FORMAT (3H   F5.2,6H    F4.2,7H       F5.3,9H      F5.4,7H
   1    F5.4,6H     F5.4,5H    1PE1Ø.3,4H     ØPE12.5)
 5Ø CONTINUE
    CALL EXIT
    END
```

PROGRAM III - LIST OF SYMBOLS

Symbol	Meaning	Units
(I)+(J)	Gaussian abscissae, number (1-16)	
X(I)	Normalized Gaussian abscissae based on model length of two, from -1 to+ 1	
Y(I)	Normalized ordinate of body meridian profile	
R(I)	Gaussian weighting functions	
RO	Water density	slug/ ft^3
PATD(M)	Static pressure (gage)	PsiG
V(L,M,N)	Absolute model velocity	kts.
N	Body number	
M	Depth	
L	Speed	
AL(I)	Cosine of angle between tangent to body profile and x-axis	
A(I)	$\lambda(I)$ ratio of length to diameter	
B(I)	$k_1(I)$, longitudinal virtual mass coefficient	
G(J,I)	g(x,t), equation of prolate spheroid whose ends coincide with ends of the given body, and which intersects body at x =t.	
C(J,I)	K (x,t), matrix of functions of body	
D(J,I)	$K'(x,t)$,Matrix of functions of prolate spheroid	
SUM(I)	$\Sigma(K-K')$	
E(K,I)	E(n,t),error functions	
H(I)	$\frac{k_1 + E}{1 + k_1 (x)}$	
K	Iteration number	

PROGRAM III - (CONT'D)

Symbol	Meaning	Units
SUM(I)	$\sum(En_{nj} - E_{ni})$	
O(I)	$\sum E_{ni}$	
U(I)	v/u_∞ , ratio of flow velocity over body to free stream velocity.	
P(I)	p/q , pressure distribution	
VEL(I)	Absolute flow velocity over body	kts.
PCC(I)	Gage pressure on body	lb/ft^2

LOGICAL SEQUENCE FOR PROGRAM III

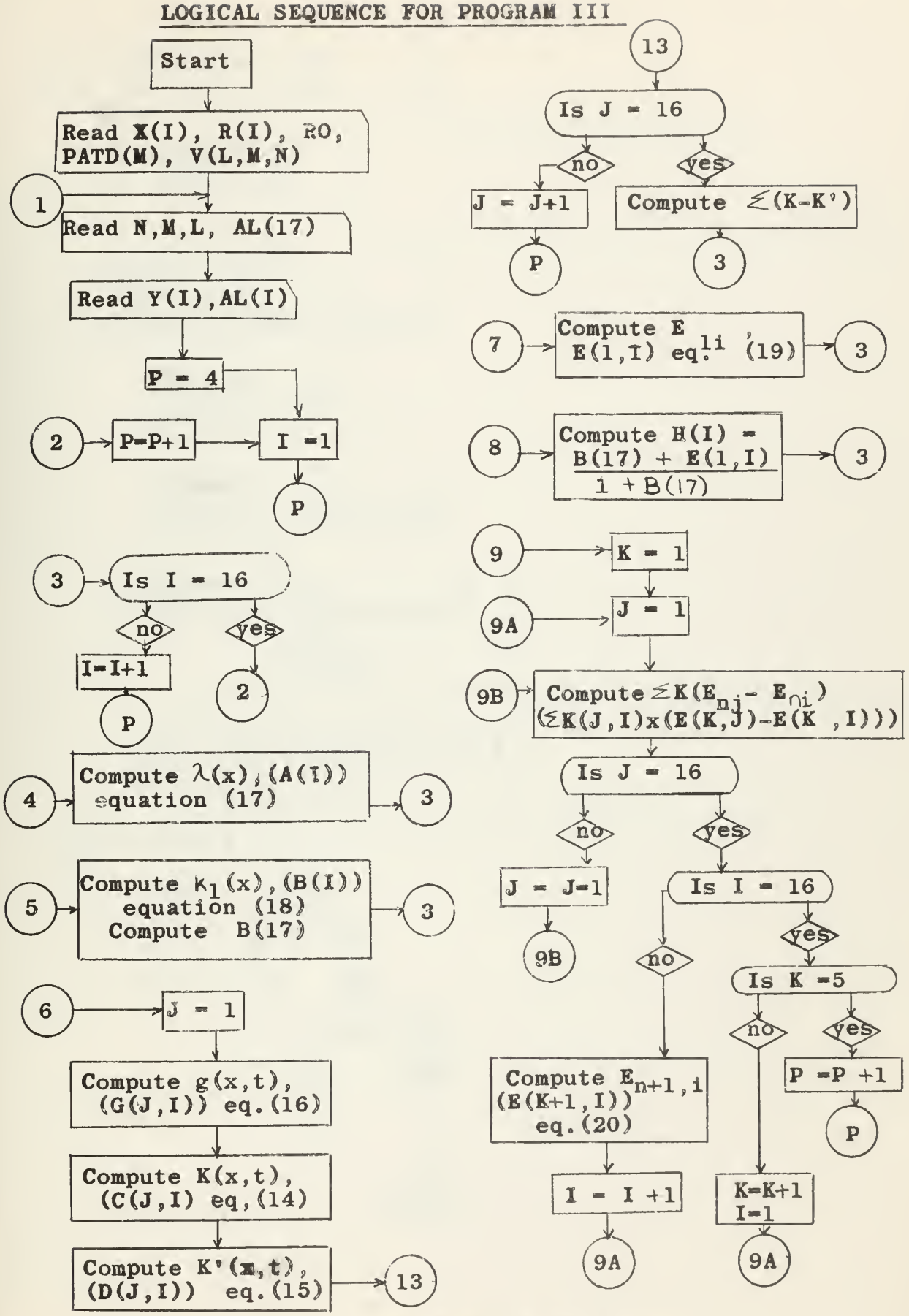

(continued on next page)

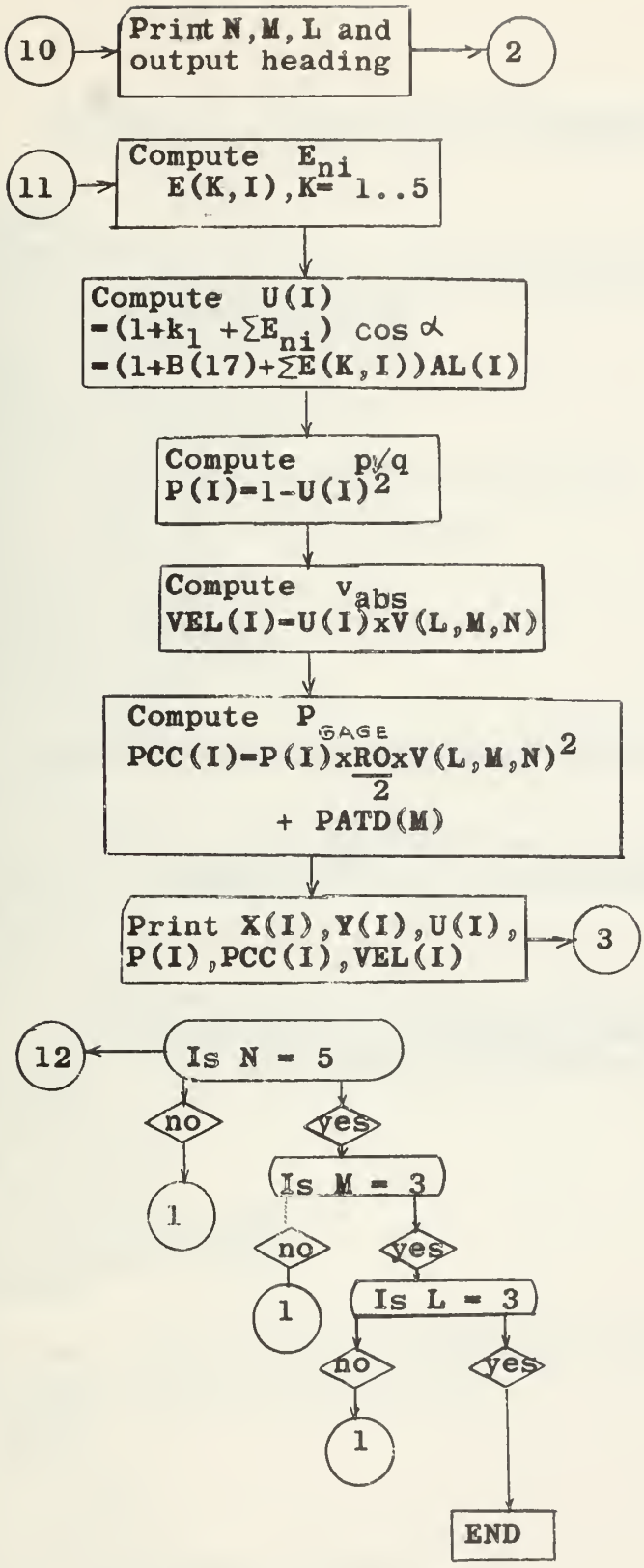
10
Print N, M, L and output heading
2
11
Compute E_{ni} E(K,I), K= 1..5
Compute U(I)
$-(1+k_1+\Sigma E_{ni})\cos\alpha$
-(1+B(17)+ΣE(K,I))AL(I)
Compute p/q
$P(I)=1-U(I)^2$
Compute v_{abs}
VEL(I)=U(I)xV(L,M,N)
Compute P_{GAGE}
$PCC(I)=P(I)x\frac{ROxV(L,M,N)^2}{2}$ + PATD(M)
Print X(I), Y(I), U(I), P(I), PCC(I), VEL(I)
3
12
Is N = 5
no
yes
1
Is M = 3
no
yes
1
Is L = 3
no
yes
1
END

PROGRAM III CALCULATION OF PRESSURE DISTRIBUTION

```
    FORTRAN
    DIMENSION X(16),R( 16),Y(16),AL(16,5),A(17),B(17),C(16,16),D(16,16)
   1,SUM(16),E(5,16),H(16),O(16),U(16),S(16),P(16),G(16,16),PATD(3),
   2V(3,3,5),VEL(16),PCC(16)
    READ 1,(X(I),R(I),I=1,16)
 1 FORMAT (6E12.5)
   READ2,RO,(PATD(M),M=1,3)
 2 FORMAT(F5.3,3E11.4)
   READ3,(((V(L,M,N),L=13),M=1,3),N=1,5)
 3 FORMAT (18F4.2)
   READ7,((AL(I,N),I=1,16),N=1,5)
 7 FORMAT(14F5.3)
 4 READ5,N,M,L,A(17)
 5 FORMAT(3I1,E12.5)
  READ6,(Y(I),I=1,16)
 6 FORMAT(6E12.5)
   DO 1Ø I=1,16
   A(I)=SQRTF((X(I)+1.)*(1.-X(I))/(Y(I)**2.))
1Ø CONTINUE
   DO 2Ø I=1,17
   B(I)=(A(I)*LOGF(A(I)+SQRTF(A(I)** 2.-1.))-SQRTF(A(I)**2.-1.))/
   1((A(I)**2.)*SQRTF(A(I)**2.-1.)-A(I)*LOGF(A(I)+SQRTF(A(I)**2.-1.)))
2Ø CONTINUE
   DO 3Ø I=1,16
   DO 3Ø J=1,16
   G(J,I)=(Y(I)**2.)*(X(J)+1.)*(1.-X(J))/((X(I)+1.)*(1.-X(I)))
   C(J,I)=R(J)*(Y(J)**2.)/(((X(J)-X(I))**2.+Y(J)**2.)**1.5)
   D(J,I)=R(J)*G(J,I)/(((X(J)-X(I))**2.+G(J,I))**1.5)
3Ø CONTINUE
   DO 4Ø I=1,16
   SUM(I)=Ø.Ø
   DO 39 J=1,16
   S(J)=C(J,I)-D(J,I)
   SUM(I)=SUM(I)+S(J)
39 CONTINUE
   K=1
   E(K,I)=1.-(((1.+B(17))/2.)*SUM(I))-(1.+B(17))/(1.+B(I))
   H(I)=(E(K,I)+B(17))/(1.+B(17))
4Ø CONTINUE
   DO 5Ø K=1,4
   DO 5Ø I=1,16
   SUM(1)=Ø.Ø
   DO 49 J=1,16
   S(J)=C(J,I)*(E(K,J)-E(K,I))
   SUM(I)= SUM(I) + S(J)
49 CONTINUE
```

PROGRAM III (CONT"D)

```
   E(K+1,I)=H(I)*E(K,I)-.5*SUM(I)
5Ø CONTINUE
   PRINT 52,N
52 FORMAT(14H2 BODY NUMBER=I1)
   PRINT53,M
53 FORMAT (8HØ DEPTH=I1)
   PRINT54,V(L,M,N)
54 FORMAT (8HØ SPEED=F4.2)
   PRINT55
55 FORMAT (83HØ        X(I)          Y(I)          U(I)        P(I)
   1         PCC(I)              VEL(I)/)
   DO 6Ø I=1,16
   0(I)=E(1,I)+E(2,I)+E(3,I)+E(4,I)+E(5,I)
   U(I)=(1.+B(17)+0(I))*AL(I,N)
   P(I)=1.-(U(I))**2.
   VEL(I)=U(I)*V(L,M,N)
   PCC(I)=P(I)*(.5*RO*((V(L,M,N)*1.689)**2.))+PATD(M)*144.
57 PRINT 59, (X(I),Y(I),U(I),P(I),PCC(I),VEL(I))
59 FORMAT(6E14.5)
6Ø CONTINUE
   GO TO (4,4,4,4,61),N
61 GO TO (4,4,62),M
62 GO TO (4,4,63),L
63 CALL EXIT
   END
```

APPENDIX D - EXPERIMENTAL DATA

TABLE D-I - EXPERIMENTAL DRAG DATA

Run	Stern	Depth	Dial Speed	Speed (KTS)	Voltmeter Zero(V)	Voltmeter AVG (V)	Voltmeter Diff.(V)	Measured Drag(lbs)
1	3	1	20	0.80	-43.7	-26.4	17.3	0.21
1A	↑	↑	20	0.77	-45.0	-27.9	17.1	0.21
2	|	|	24	1.12	-46.5	-20.4	26.1	0.33
2A	|	|	24	1.12	-45.7	-18.5	27.2	0.34
3	|	↓	28	1.48	-45.0	-14.75	30.25	0.38
3A	|	1	28	1.48	-43.5	-11.7	31.8	0.40
4	|	2	20	0.75	-45.1	-29.2	15.9	0.20
4A	3	↑	20	0.74	-47.7	-30.8	16.9	0.21
5	|	|	24	1.09	-45/5	-22.6	22.9	0.24
5A	|	|	24	1.09	-44.7	-18.5	26.2	0.33
6	|	↓	28	1.50	-43.0	-18.4	24.6	0.31
6A	|	2	28	1.51	-43.5	-19.0	24.5	0.31
7	|	3	20	0.77	-46.0	-30.7	15.3	0.19
7A	|	↑	20	0.79	-46.1	-30.9	15.2	0.19
8	|	|	24	1.16	-45.5	-23.6	21.9	0.27
8A	|	|	24	1.17	-45.0	-25.1	19.9	0.25
9	↓	↓	28	1.62	-46.0	-19.6	26.4	0.33
9A	3	3	28	1.58	-45.0	-21.0	24.0	0.30
10	1	3	20	0.77	-45.0	-23.2	21.8	0.28
10A	↑	↑	20	0.77	-46.0	-21.2	25.0	0.31
11A	|	|	24	1.16	-46.0	-24.0	22.0	0.28
11B	|	|	24	1.21	-46.5	-25.8	20.7	0.26
12	|	↓	28	1.58	-46.0	-19.7	26.3	0.33
12A	|	3	28	1.58	-45.5	-20.0	25.5	0.32
13	|	2	20	0.75	-35.0	-22.6	12.4	0.16
13A	|	↑	20	0.75	-36.0	-24.2	11.8	0.15
14	1	|	24	1.19	-35.0	-13.2	21.8	0.28
14A	|	|	24	1.11	-37.5	-15.2	22.3	0.28
15	|	↓	28	1.61	-42.5	-12.5	30.0	0.38
15A	|	2	28	1.61	-44.0	-12.6	31.4	0.39
16	|	1	20	0.74	-25.0	-15.4	09.6	0.12
16A	|	↑	20	0.74	-26.7	-16.1	10.6	0.13
17	|	|	24	1.13	-39.0	-16.1	22.8	0.28
17A	|	|	24	1.16	-40.5	-15.2	25.3	0.31
18	↓	↓	28	1.56	-44.0	-09.2	34.8	0.44
18A	1	1	28	1.53	-46.0	-12.6	33.4	0.42

TABLE D-I (CON'T) EXPERIMENTAL DATA

Run	Stern	Depth	Dial Speed	Speed (KTS)	Voltmeter Zero(V)	Voltmeter AVG (V)	Voltmeter Diff.(V)	Measured Drag(lbs)
19	2	1	20	0.75	-44.0	-28.6	15.4	0.19
19A	↑	↑	20	0.73	-45.0	-29.4	15.6	0.20
20	|	|	24	1.14	-46.0	-20.0	26.0	0.32
20A	|	|	24	1.16	-46.5	-17.9	28.6	0.36
21	|	↓	28	1.61	-44.5	-13.2	31.3	0.39
21A	|	1	28	1.56	-43.5	-17.9	25.6	0.32
22	|	2	20	0.80	-24.0	-09.3	14.7	0.16
22A	2	↑	20	0.73	-24.5	-11.3	13.2	0.14
23	|	|	24	1.15	-28.0	-09.0	19.0	0.21
23A	|	|	24	1.14	-26.0	-07.5	18.5	0.21
24	|	↓	28	1.67	-25.0	-04.6	20.4	0.23
24A	|	2	28	1.60	-24.5	-04.0	20.5	0.23
25	|	3	20	0.73	-37.0	-13.2	23.8	0.28
25A	|	↑	20	0.75	-33.0	-10.3	22.7	0.26
26	|	|	24	1.18	-32.0	-09.4	22.6	0.26
26A	|	|	24	1.18	-30.0	-07.6	22.4	0.26
27	↓	↓	28	1.53	-29.0	-05.5	23.5	0.27
27A	2	3	28	1.50	-26.0	-03.8	22.8	0.26
28	4	3	20	0.70	-40.0	-08.6	21.4	0.25
28A	↑	↑	20	0.70	-42.5	-17.5	25.0	0.29
29	|	|	24	1.00	-45.0	-19.2	25.8	0.31
29A	|	|	24	1.25	-42.5	-16.2	26.3	0.31
30	|	↓	28	1.65	-40.0	-11.2	28.8	0.35
30A	|	3	28	1.67	-40.0	-11.2	28.8	0.35
31	|	2	20	0.78	-35.0	-17.2	17.8	0.20
31A	|	↑	20	0.78	-34.5	-15.7	18.8	0.21
32	4	|	24	1.22	-31.5	-08.8	22.7	0.26
32A	|	|	24	1.23	-32.0	-10.0	22.0	0.25
33	|	↓	28	1.63	-32.0	-07.4	24.6	0.29
33A	|	2	28	1.58	-30.0	-05.2	24.8	0.30
34	|	1	20	0.77	-43.0	-19.7	23.3	0.26
34A	|	↑	20	0.76	-48.0	-24.1	23.9	0.28
35	|	|	24	1.20	-47.0	-15.2	31.8	0.39
35A	|	|	24	1.18	-40.5	-12.3	28.2	0.34
36	↓	↓	28	1.58	-41.0	-05.4	35.6	0.45
36A	4	1	28	1.58	-44.0	-07.7	36.3	0.45
37	5	1	20	0.78	-37.0	-18.1	18.9	0.21
37A	↑	↑	20	0.80	-44.0	-20.9	23.1	0.27
38	|	|	24	1.21	-30.5	-05.0	25.5	0.30
38A	|	|	24	1.18	-34.5	-06.2	28.3	0.34

TABLE D-I(CONT'D) EXPERIMENTAL DATA

Run	Stern	Depth	Dial Speed	Speed (KTS)	Voltmeter Zero (V)	Voltmeter AVG (V)	Voltmeter Diff.(V)	Measured Drag(lbs)
39		↓	28	1.67	-37.5	-01.1	36.4	0.46
39A		1	28	1.80	-43.0	-07.3	35.7	0.44
40		2	20	0.80	-45.0	-20.1	24.9	0.29
40A	5	↑	20	0.80	-46.0	-20.3	25.7	0.30
41			24	1.28	-46.5	-15.3	31.2	0.38
41A			24	1.28	-46.0	-13.5	32.5	0.40
42		↓	28	1.70	-46.0	- 8.8	37.2	0.47
42A		2	28	1.65	-46.0	- 8.4	37.6	0.47
43		3	20	0.75	-43.5	-18.1	25.4	0.30
43A		↑	20	0.75	-39.5	-17.3	22.2	0.26
44			24	1.25	-39.0	-14.4	24.6	0.29
44A			24	1.28	-38.5	-13.1	25.4	0.30
45	↓	↓	28	1.63	-37.0	-07.4	29.6	0.35
45A	5	3	28	1.60	-36.0	-07.0	29.0	0.35

Depth 1 = 18" to Keel (4.5×Dia.)
Depth 2 = 10" to Keel (2.5×Dia.)
Depth 3 = 3.6"to Keel (0.9×Dia.)

Runs - 1 - 21A Conducted 24 March 1962
22 - 45A Conducted 25 March 1962

Water Temp = 51° F

$\nu = 1.386 \times 10^{-5}$ ft^2/sec

$\rho = 1.939$ lb - sec^2/ft^4

Dial speed is setting on manual speed control knob.

TABLE D-II - SEPARATION POINT DATA

Run	Stern	Run Classification	Separation Point	Body Angle
1	3	LD	5.0″	33°
1A	↑	LD	5.0	33
2	|	MD	5.0	33
2A	|	MD	5.0	33
3	|	HD	5.0	33
3A	|	HD	5.0	33
4	|	LM	4.75	28
4A	|	LM	4.75	28
5	|	MM	4.75	28
5A	|	MM	4.75	28
6	|	HM	4.75	28
6A	|	HM	5.0	33
7	|	LS	4.5	23
7A	|	LS	4.5	23
8	|	MS	4.5	23
8A	|	MS	4.5	23
9	↓	HS	4.75	28
9A	3	HS	4.5	23
10	1	LS	0.8	24
10	↑	LS	0.8	24
11A	|	MS	1.25	42
11B	|	MS	1.25	42
12	|	HS	1.3	42
12A	|	HS	1.35	42
13	|	LM	0.75	24
13A	|	LM	0.75	24
14	|	MM	1.0	32
14A	|	MM	1.1	32
15	|	HM	1.1	32
15A	|	HM	1.1-1.2	32
16	|	LD	0.8-09	24
16A	|	LD	0.8	24
17	|	MD	0.8	24
17A	|	MD	0.8-0.9	24
18	↓	HD	1.3	42
18A	1	HD	1.3	42
19	2	LD	2.75	30
19A	↑	LD	2.5	25
20	|	MD	3.0	36
20A	|	MD	3.1	36
21	|	HD	?	-
21A	|	HD	3.0	36

TABLE D-II (cont'd)

Run	Stern	Run Classification	Separation Point	Body Angle
22		LM	3.0"	36°
22A		LM	2.6	25
23		MM	2.6	30
23A		MM	2.8	30
24		HM	?	-
24A		HM	2.75	30
25		LS	2.9	33
25A		LS	2.8	30
26		MS	3.1	36
26A		MS	3.2	42
27		HS	3.3	42
27A	2	HS	3.25	42
28	4	LS	7.0	38
28A		LS	7.0	38
29		MS	7.1	44
29A		MS	7.1	44
30		HS	7.3	49
30A		HS	7.3	49
31		LM	7.1	44
31A		LM	7.1	44
32		MM	7.2	49
32A		MM	7.2	49
33		HM	7.2	49
33A		HM	7.2	49
34		LD	6.8	28
34A		LD	6.7	28
35		MD	6.8	28
35A		MD	6.9	30
36		HD	7.0	38
36A	4	HD	?	-
37	5	LD	10.5?	23
37A		LD	?	-
38		MD	10.5	23
38A		MD	10.5	23
39		HD	10.5	23
39A		HD	10.5	23
40		LM	11.0	30
40A		LM	11.0	30
41		MM	?	-
41A		MM	?	-
42		HM	10.9	30
42A		HM	?	-
43		LS	?	-
43A		LS	?	-
44		MS	11.5	60
44A		MS	11.5	60
45		HS	11.5	60
45A	5	HS	11.5	60

TABLE D-II (Cont'd)

NOTE:

Run classification code - 1st letter designates speed

L = low
M = medium
H = high

2nd letter designates depth

D = depth 1 (deep)
M = depth 2 (medium)
S = depth 3 (surfaced)

Separation point is measured in inches from end of cylindrical section. Marks on photographs are $\frac{1}{2}$ inch apart.

Body angle is angle between body axis and body surface at separation point.

APPENDIX E - DISCUSSION OF DRAG FORCE MEASUREMENTS

The experimental data from Table D-I was reduced to coefficient form using the following procedure.

(Drag measured) - (Strut drag) = (Total corrected drag)

where strut drag was calculated by the method that follows. Measurement of a strut tare drag was attempted but due to either the end effects on the strut because of the lack of a dummy body or faulty instrumentation these values were of a larger magnitude than the values of measured drag of the body plus strut and thus were not valid. An engineering value of strut drag composed of profile drag, spray drag, wave drag, and interference drag with the body was calculated as follows:

Profile Drag:

$$t/_c = \frac{.8}{3.25} = .246 \quad \text{for strut used.}$$

Reynold Number on Strut $\cong 3 \times 10^4$

from figure 126, page 247 of [9]

$Cd \cong 0.08$

$$\text{Drag} = q \frac{Cd\,(.8 \times SL)}{144} = q \frac{(.064)\,SL}{144}$$

where SL = strut length submerged (inches)

$$q = \frac{1}{2} \rho V_k^2 \left(1.689\right)^2$$

Spray Drag:

Froude number on strut $\approx 4 \times 10^{-1}$

$$\frac{t}{2x} = \frac{.8}{3.25} = .246$$

from figure 25, page 10-13 of [10]

$$Cd_x = .24 \left(\frac{t}{x}\right)^2 = .058 \qquad x = 1.625$$

$$\text{Drag} = q\ Cd_x(X^2) = \frac{q}{144}\ (.1535)$$

Wave Drag:

from figure 24, page 10-13 of (10)

$$Cd_t \approx 1.4$$

$$\text{Drag} = q\ Cd_t\ t^2 = \frac{q}{144}\ (.895)$$

Interaction Drag:

from figure 23, page 8-10 of (10)

$$C_{dt} = .75 \times t/c = .19$$

$$\text{Drag} = C_{d_t}\ q\ t^2 = \frac{q}{144}\ (.121)$$

Total Strut Drag:

$$\text{Strut Drag} = \frac{1}{2} \rho\ V_K^2\ \frac{(1.689)^2}{144} \left[.064SL + 1.17\right] \qquad (27)$$

The total corrected drag was converted to coefficient form by the following relationship:

$$C_t = \frac{\text{Drag}}{1/2\ \rho\ V_K^2\ (1.689)^2\ (S)} \qquad (28)$$

where S = wetted surface of the model.

The coefficient of frictional resistance, C_f, was next calculated using Schoenherr's relationship that:

$$C_f = 0.0585 \left[\log_{10}\ (R_n C_f)\right]^{-2}$$

$$= \frac{0.0585}{\left[.4343\ \log_e\ (Rn\ C_f)\right]^2} \qquad (29)$$

In order to use the electronic computer to evaluate (29), the Schultz-Grunow formulation

$$C_f = 0.0725 \left[\log_{10} Rn - 2.0\right]^{-2}$$

$$= \frac{0.0725}{\left[.4343 \log_e R_n - 2.0\right]^2} \qquad (30)$$

which yields Cf values greater than that of (29) in the range of interest in this problem was calculated and used as a first value to solve (29) which is implicit in Cf.

The residual resistance coefficient, C_r, was then calculated from:

$$C_r = C_t - C_f \qquad (31)$$

It was hoped that perhaps some correlation between the change of location of separation on the body and change in C_r for various runs could be found if our drag measurements were good.

An IBM 7090 comuter program, Program I was written to solve equations (27) through (31). The details of this program are given in Appendix C. Sample outputs of this program are included in Table E-I at the end of this appendix. These values which are typical of the values obtained on all the bodies are much too large for the underwater shapes tested. At submerged depth 1 the values of Cr and C_t are over ten times as large as would be expected by comparison to Series 58 data.

At first strut drag was suspected but in the surfaced condition where strut drag does not enter into the calculation the residual drag values are much too large also. The bow waves generated in the surfaced condition are shown in Figure IX. It is not possible for the wave making resistance created in this

condition to account for such large values of C_r. Besides being too large in magnitude the values are not consistent from body to body with the highly streamlined body sometimes showing a higher C_r value than a less streamlined body for similar speed and depth of submergence. Plots of C_r versus both Reynolds number and speed-length ratio were prepared but these were completely inconsistent and unsatisfactory when compared to similar plots of similar bodies in the literature.

At the time of this writing the cause of the excess drag is unknown. It is speculated that the dynamic response of the drag measuring system is causing a false reading of drag due to some phenomena that does not appear during static calibration. The calibration curves used in this work are shown in Figure E-I. It is also of interest that another group using another submerged model experienced the same difficulty, i.e., too much drag.

If it is desired to make further drag measurements on the model it is recommended that the drag force dynamometer be mounted at the model rather than in the strut. This will eliminate the problem relating to strut drag with the exception of the interference drag between the strut and body. It is also recommended that the dynamic response of the entire drag measuring system used during the tests be given a thorough investigation. The authors realize that

the new towing tank and dynamometer equipment was put to use on an emergency basis, the construction of such apparatus being completed, and before the carriage and instrumentation were properly calibrated, accepted, and put into regular use. Upon completion of all of these steps it should be feasible to carry out successful drag measurements on submerged bodies at the new M.I.T. Towing Tank.

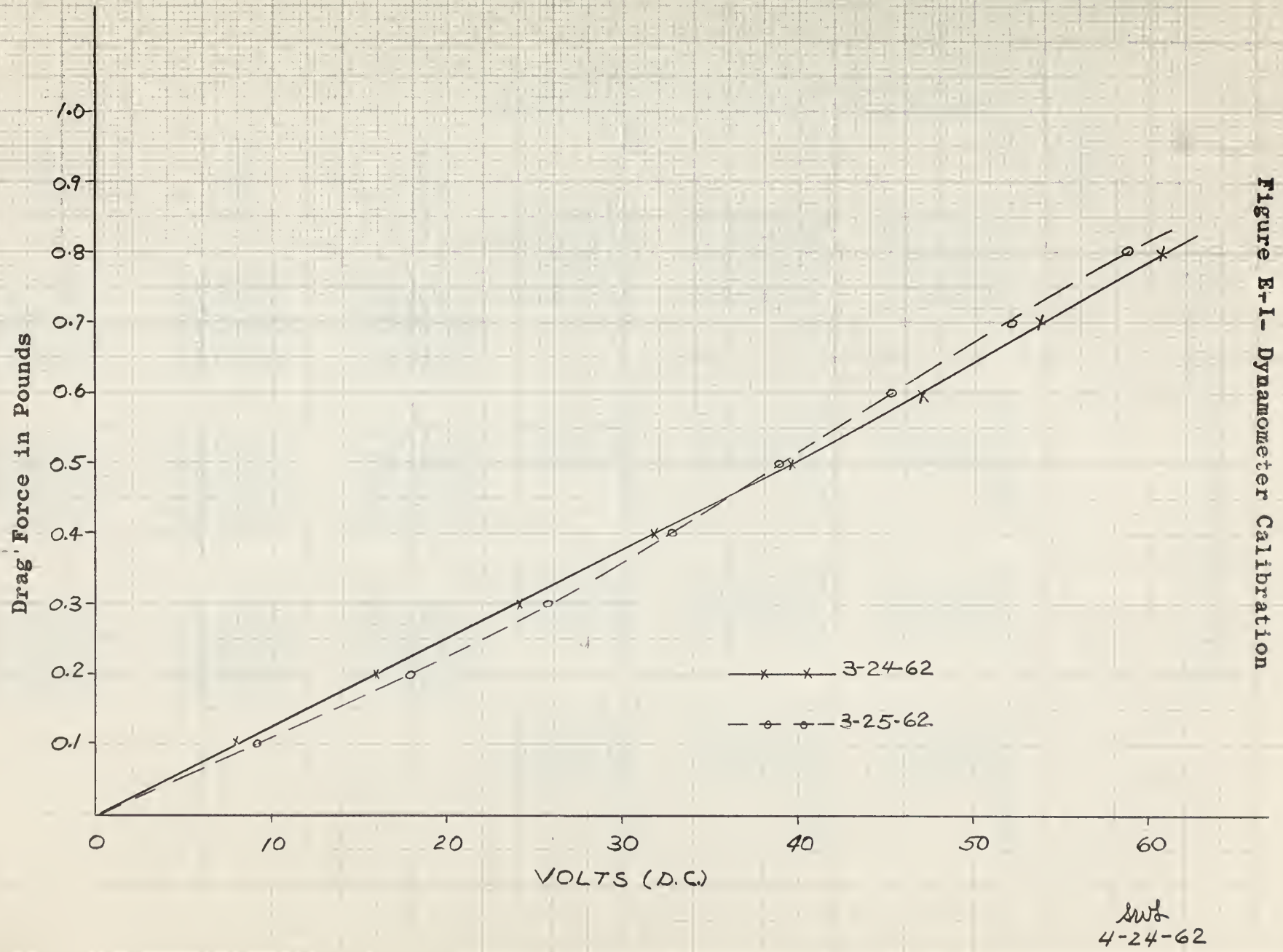

Figure E-I- Dynamometer Calibration

TABLE E-I - SAMPLES OF COMPUTER OUTPUT, PROGRAM I

BODY NUMBER=1

DEPTH=1

VEL.(KT.	REYNOLDS NO.	SPEED/LENGTH	TOT.DRAG	TOT.DRAG(CORR)
0.74	2.372E 05	0.46	0.120	0.098
0.74	2.372E 05	0.46	0.130	0.108
1.13	3.622E 05	0.70	0.280	0.229
1.16	3.718E 05	0.72	0.310	0.257
1.56	5.000E 05	0.96	0.440	0.343
1.53	4.904E 05	0.94	0.420	0.327

DEPTH=2

VEL.(KT.	REYNOLDS NO.	SPEED/LENGTH	TOT.DRAG	TOT.DRAG(CORR)
0.75	2.404E 05	0.46	0.160	0.143
0.75	2.404E 05	0.46	0.150	0.133
1.19	3.814E 05	0.73	0.280	0.238
1.11	3.558E 05	0.68	0.280	0.243
1.61	5.160E 05	0.99	0.380	0.303
1.61	5.160E 05	0.99	0.390	0.313

DEPTH=3

VEL.(KT.	REYNOLDS NO.	SPEED/LENGTH	TOT.DRAG	TOT.DRAG(CORR)
0.77	2.468E 05	0.47	0.280	0.280
0.77	2.468E 05	0.47	0.310	0.310
1.16	3.718E 05	0.72	0.280	0.280
1.21	3.878E 05	0.75	0.260	0.260
1.58	5.064E 05	0.97	0.330	0.330
1.58	5.064E 05	0.97	0.320	0.320

	CT	CF	CR
	2.541E-02	5.909E-03	1.950E-02
	2.799E-02	5.909E-03	2.208E-02
DEPTH = 1	2.543E-02	5.400E-03	2.003E-02
	2.700E-02	5.371E-03	2.163E-02
	1.998E-02	5.053E-03	1.493E-02
	1.978E-02	5.073E-03	1.471E-02

	CT	CF	CR
	3.604E-02	5.892E-03	3.015E-02
	3.353E-02	5.892E-03	2.763E-02
DEPTH = 2	2.377E-02	5.342E-03	1.842E-02
	2.795E-02	5.421E-03	2.253E-02
	1.653E-02	5.021E-03	1.151E-02
	1.707E-02	5.021E-03	1.205E-02

	CT	CF	CR
	7.797E-02	5.858E-03	7.211E-02
	8.632E-02	5.858E-03	8.047E-02
DEPTH = 3	3.436E-02	5.371E-03	2.898E-02
	2.932E-02	5.324E-03	2.400E-02
	2.182E-02	5.040E-03	1.678E-02
	2.116E-02	5.040E-03	1.612E-02

TABLE E-I (CON'T)

BODY NUMBER=3

DEPTH=1

VEL.(KT.	REYNOLDS NO.	SPEED/LENGTH	TOT.DRAG	TOT.DRAG(CORR)
0.80	2.856E 05	0.47	0.210	0.185
0.77	2.749E 05	0.45	0.210	0.186
1.12	3.999E 05	0.65	0.330	0.280
1.12	3.999E 05	0.65	0.340	0.290
1.48	5.284E 05	0.86	0.380	0.293
1.48	5.284E 05	0.86	0.400	0.313

DEPTH=2

VEL.(KT.	REYNOLDS NO.	SPEED/LENGTH	TOT.DRAG	TOT.DRAG(CORR)
0.75	2.678E 05	0.44	0.200	0.183
0.74	2.642E 05	0.43	0.210	0.194
1.09	3.892E 05	0.64	0.290	0.255
1.09	3.892E 05	0.64	0.330	0.295
1.50	5.356E 05	0.88	0.310	0.243
1.51	5.392E 05	0.88	0.310	0.242

DEPTH=3

VEL.(KT.	REYNOLDS NO.	SPEED/LENGTH	TOT.DRAG	TOT.DRAG(CORR)
0.77	2.749E 05	0.45	0.190	0.190
0.79	2.821E 05	0.46	0.190	0.190
1.16	4.142E 05	0.68	0.270	0.270
1.17	4.178E 05	0.68	0.250	0.250
1.62	5.784E 05	0.95	0.330	0.330
1.58	5.641E 05	0.92	0.300	0.300

	CT	CF	CR
DEPTH = 1	3.771E-02	5.678E-03	3.203E-02
	4.111E-02	5.724E-03	3.539E-02
	2.920E-02	5.290E-03	2.391E-02
	3.024E-02	5.290E-03	2.495E-02
	1.749E-02	4.997E-03	1.249E-02
	1.868E-02	4.997E-03	1.369E-02

	CT	CF	CR
DEPTH = 2	4.258E-02	5.756E-03	3.682E-02
	4.623E-02	5.773E-03	4.046E-02
	2.801E-02	5.320E-03	2.269E-02
	3.241E-02	5.320E-03	2.709E-02
	1.411E-02	4.983E-03	9.126E-03
	1.387E-02	4.976E-03	8.894E-03

	CT	CF	CR
DEPTH =3	5.058E-02	5.724E-03	4.485E-02
	4.805E-02	5.693E-03	4.235E-02
	3.167E-02	5.252E-03	2.642E-02
	2.882E-02	5.243E-03	2.358E-02
	1.985E-02	4.906E-03	1.494E-02
	1.897E-02	4.931E-03	1.403E-02

TABLE E-I (CON'T.)

BODY NUMBER=5

DEPTH=1

VEL.(KT.	REYNOLDS NO.	SPEED/LENGTH	TOT.DRAG	TOT.DRAG(CORR)
0.78	3.241E 05	0.42	0.210	0.186
0.80	3.324E 05	0.43	0.270	0.245
1.21	5.028E 05	0.66	0.300	0.242
1.18	4.903E 05	0.64	0.340	0.285
1.67	6.940E 05	0.90	0.460	0.349
1.80	7.480E 05	0.97	0.440	0.311

DEPTH=2

VEL.(KT.	REYNOLDS NO.	SPEED/LENGTH	TOT.DRAG	TOT.DRAG(CORR)
0.80	3.324E 05	0.43	0.290	0.271
0.80	3.324E 05	0.43	0.300	0.281
1.28	5.319E 05	0.69	0.380	0.331
1.28	5.319E 05	0.69	0.400	0.351
1.70	7.064E 05	0.92	0.470	0.384
1.65	6.857E 05	0.89	0.470	0.389

DEPTH=3

VEL.(KT.	REYNOLDS NO.	SPEED/LENGTH	TOT.DRAG	TOT.DRAG(CORR)
0.75	3.117E 05	0.41	0.300	0.300
0.75	3.117E 05	0.41	0.260	0.260
1.25	5.194E 05	0.68	0.290	0.290
1.28	5.319E 05	0.69	0.300	0.300
1.63	6.773E 05	0.88	0.350	0.350
1.60	6.649E 05	0.87	0.350	0.350

	CT	CF	CR
	3.540E-02	5.528E-03	2.987E-02
	4.429E-02	5.498E-03	3.879E-02
DEPTH = 1	1.915E-02	5.047E-03	1.410E-02
	2.370E-02	5.073E-03	1.863E-02
	1.452E-02	4.731E-03	9.785E-03
	1.114E-02	4.662E-03	6.478E-03

	CT	CF	CR
	4.905E-02	5.498E-03	4.355E-02
	5.086E-02	5.498E-03	4.537E-02
DEPTH = 2	2.342E-02	4.990E-03	1.843E-02
	2.483E-02	4.990E-03	1.984E-02
	1.539E-02	4.714E-03	1.067E-02
	1.655E-02	4.742E-03	1.181E-02

	CT	CF	CR
	7.374E-02	5.574E-03	6.817E-02
	6.391E-02	5.574E-03	5.834E-02
DEPTH = 3	2.566E-02	5.014E-03	2.065E-02
	2.532E-02	4.990E-03	2.033E-02
	1.821E-02	4.754E-03	1.346E-02
	1.890E-02	4.771E-03	1.413E-02

APPENDIX F - SAMPLE CALCULATIONS

Calculation of Hydrostatic Pressure.

The hydrostatic pressure to the keel of the bodies at the three depths of submergence is desired for use in computer Program III to compute the gage pressure on the body from the following relationship:

$$P_{gage} = \left(\frac{P}{q}\right) q + P_s \ (144)$$

where P = dynamic pressure (psf)

$q = 1/2\ \rho U^2$ (psf)

P_s = hydrostatic pressure (psi)

$$P_s = \frac{\rho g h}{1728}$$

where $\rho = 1.935 \ \frac{lb.sec^2}{ft^4}$ at $51^\circ F$

$g = 32.174 \ ft/sec^2$

h = depth to keel (inches)

Using the foregoing relation the following results were obtained:

Depth	h(inches)	Ps(psi)
1	18	.6484
2	10	.3602
3	3.6	.1297

Calculation of Point of Separation from Stratford Criterion

A typical calculation of the location of the separation point according to Stratford's criterion is given below for body #3 at velocity of 0.75 knots.

From the form of (21) separation can occur only when Cp , as plotted in Figure F-II, is positive since negative values of Cp will result in imaginary numbers.

At X = 34.8" $\frac{X}{L} = \frac{34.8}{35.15} = 0.99$

from Figure F-I; $\frac{U}{U\infty} = 0.75$

from Table G-I; Reynolds number = 2.65×10^5 at X=34.8"

thus $Rs = .75\ (2.65 \times 10^5) = 1.99 \times 10^5$

from Figure F-II; Cp = 0.05 and $\frac{dCp}{dx} = 0.50$

n = log 10 Rs = 5.30 from (22)

since, $\frac{d^2p}{dx^2} \geq 0$; $\beta = .73$ from (24)

thus the left hand side of (21) becomes

$(2x.05)^{\frac{5.30-2}{4}}\ (34.8 \times .50)^{\frac{1}{2}} = .625$

while the right hand side of (21) becomes

$(1.06)(.73)(1.99 \times 10^{-5} \times 10^6)^{-1/10} = .912$. Thus the criterion is not satisfied at X = 34.8" since the RHS is much larger than LHS. Next try

X = 34.9" $\frac{X}{L} = .995$

from Figure F-II; Cp = 0.10 and $\frac{dCp}{dx}$ = 0.96

thus the LHS of (21) becomes

$(2 \times .10)^{\frac{5.30-2}{4}} (34.9 \times .96)^{\frac{1}{2}} = 1.46$ which now makes the RHS smaller than LHS so the point of separation lies between X = 34.8" and X = 34.9."

Calculations similar to the above were used to calculate the separation points on the other bodies at the various speeds. During these calculations it was noted that the criteria was insensitive to speed changes and that the same point of separation occurred for all values of speed. The points of separation according to this criterion are marked by small circles on Figure F-II.

Calculation of Point of Separation from Buri's Criterion

A typical calculation of the location of the separation point according to Buri's criterion is given below for body #3 at a velocity of 1.12 knots.

From the form of equation (26) separation will occur only when $\frac{d\left(\frac{U}{U\infty}\right)}{d\left(\frac{X}{L}\right)}$ as determined from Figure F-I is negative.

at $\frac{X}{L}$ = .906;

$\frac{d\left(\frac{U}{U\infty}\right)}{d\left(\frac{X}{L}\right)} = -.115$ and $\frac{U}{U\infty} = 1.103$; from Figure F-I

and $\theta = .091$; from Table G-I

thus the left hand side of (26) becomes

$$-(.115)(1.103)(.906)(091) = -.0105 > -.006$$

Thus the point of separation lies slightly forward of $\frac{X}{L} = .906$ but in the region of where

$\frac{d\left(\frac{U}{U\infty}\right)}{d\left(\frac{X}{L}\right)}$ is still negative. Separation point is at

$\frac{X}{L} = .900$ or $X = 31.7$ inches which is as close as the point can be calculated within the accuracy of the plot in Figure F-I.

Calculations similar to the above were used to calculate the separation points on other bodies at various speeds. During these calculations it was noticed that the criterion was insensitive to speed changes and that the same point of separation occurred for all values of speed. The points of separation according to this criterion are marked by small circles on Figure F-I.

NOTE:

Figures F-I and F-II on the next two pages were plotted from values obtained from the outputs of Programs II and III as aids to evaluate (21) and (26).

FIGURE F-I - PLOT OF $\frac{U}{U_\infty}$ vs $\frac{X}{L}$

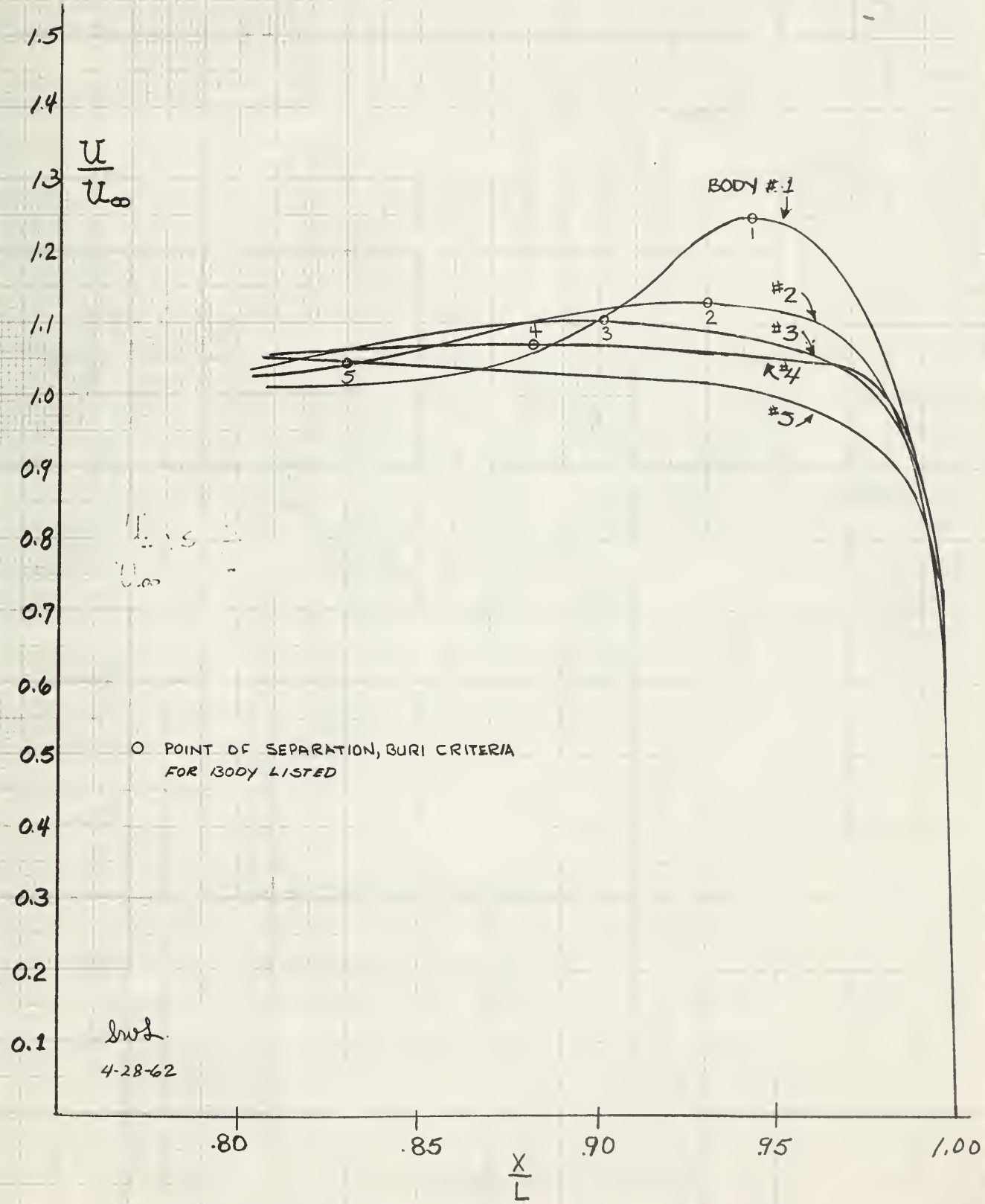

4-28-62

FIGURE F-II - Plot of C_p vs X (distance from body nose)

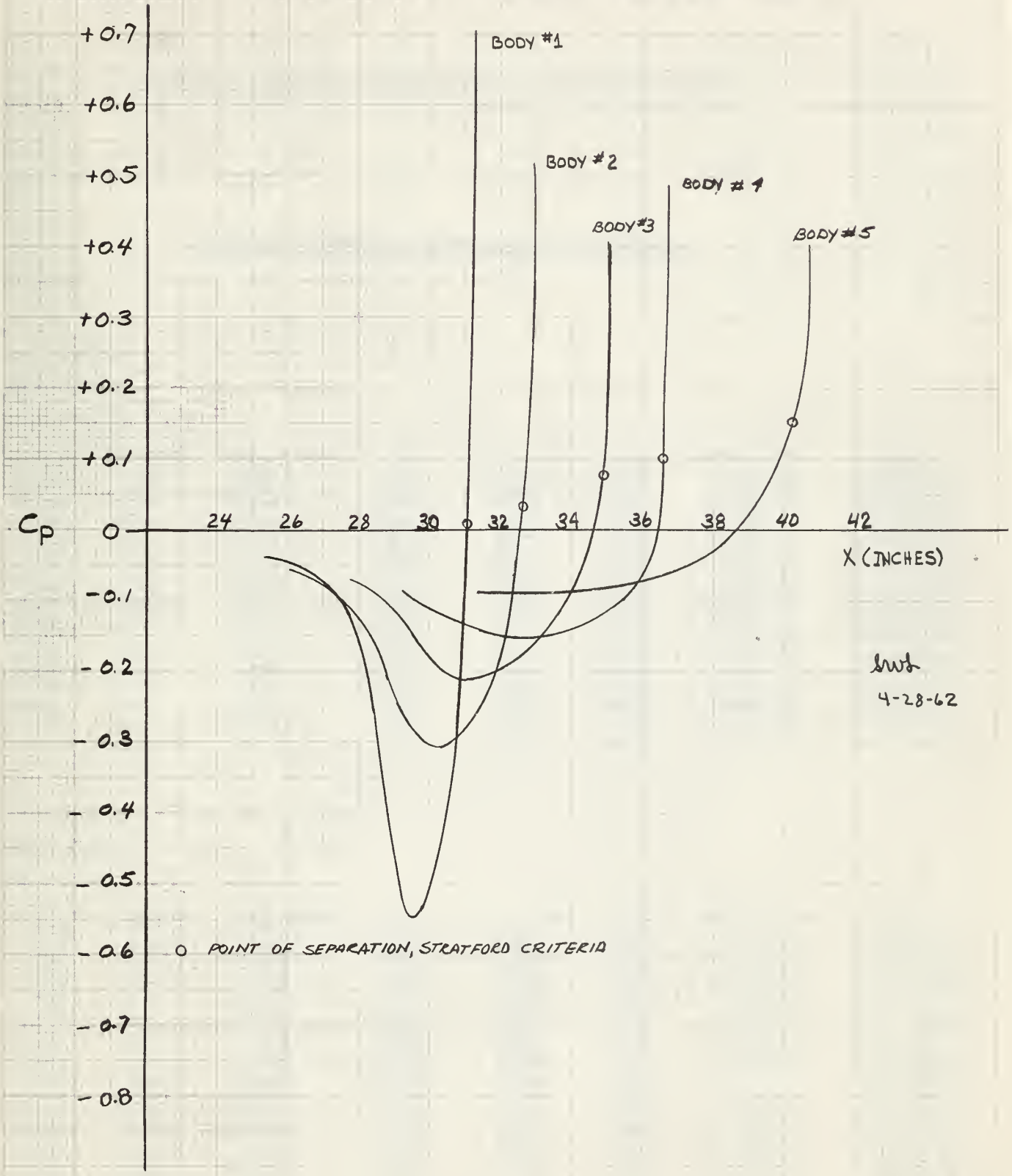

APPENDIX G - SAMPLES OF COMPUTER OUTPUT, PROGRAMS II and III

TABLE G-I - SAMPLES OF COMPUTER OUTPUT, PROGRAM II

BODY NUMBER=3

BODY DEPTH=1

VELOCITY(KTS)=1.12

X(INCH)	RADIUS	CORR. RADIUS	DELTA	DELTA-STAR	THETA	REYNOLDS NO.	Y-NORM/
0.19	0.40	0.401	.0154	.0019	.0015	2.161E 03	0.22825E-01
0.97	0.94	0.946	.0564	.0068	.0056	1.103E 04	0.53822E-01
2.36	1.37	1.383	.1141	.0135	.0114	2.684E 04	0.78683E-01
4.30	1.67	1.691	.1832	.0214	.0184	4.891E 04	0.96202E-01
6.72	1.87	1.900	.2599	.0298	.0263	7.643E 04	0.10806E-00
9.53	1.97	2.003	.3408	.0383	.0348	1.084E 05	0.11424E-00
12.62	2.00	2.047	.4225	.0465	.0437	1.435E 05	0.11641E-00
15.90	2.00	2.054	.5032	.0542	.0526	1.808E 05	0.11685E-00
19.24	2.00	2.061	.5806	.0613	.0614	2.188E 05	0.11725E-00
22.52	2.00	2.068	.6528	.0677	.0697	2.561E 05	0.11762E-00
25.62	2.00	2.073	.7181	.0734	.0773	2.914E 05	0.11794E-00
28.43	2.00	2.078	.7751	.0782	.0841	3.234E 05	0.11821E-00
30.85	1.94	2.021	.8206	.0814	.0899	3.509E 05	0.11497E-00
32.79	1.62	1.697	.8427	.0802	.0947	3.729E 05	0.96544E-01
34.17	1.15	1.217	.8326	.0734	.0985	3.886E 05	0.69213E-01
34.96	0.57	0.605	.7529	.0560	.1022	3.976E 05	0.34408E-01

BODY NUMBER=3

BODY DEPTH=2

VELOCITY(KTS)=1.51

X(INCH)	RADIUS	CORR. RADIUS	DELTA	DELTA-STAR	THETA	REYNOLDS NO.	Y-NORM/
0.19	0.40	0.401	.0145	.0018	.0014	2.914E 03	0.22821E-01
0.97	0.94	0.946	.0531	.0064	.0053	1.487E 04	0.53803E-01
2.36	1.37	1.383	.1076	.0128	.0107	3.619E 04	0.78642E-01
4.30	1.67	1.690	.1728	.0202	.0173	6.594E 04	0.96138E-01
6.72	1.87	1.898	.2453	.0282	.0248	1.030E 05	0.10797E-00
9.53	1.97	2.006	.3218	.0364	.0328	1.461E 05	0.11413E-00
12.62	2.00	2.044	.3991	.0442	.0411	1.935E 05	0.11628E-00
15.90	2.00	2.052	.4756	.0516	.0495	2.438E 05	0.11670E-00
19.24	2.00	2.058	.5490	.0585	.0578	2.950E 05	0.11709E-00
22.52	2.00	2.065	.6175	.0646	.0656	3.453E 05	0.11744E-00
25.62	2.00	2.070	.6795	.0701	.0728	3.929E 05	0.11775E-00
28.43	2.00	2.075	.7338	.0747	.0792	4.360E 05	0.11801E-00
30.85	1.94	2.018	.7771	.0779	.0846	4.731E 05	0.11477E-00
32.79	1.62	1.694	.7987	.0769	.0891	5.028E 05	0.96362E-01
34.17	1.15	1.214	.7905	.0706	.0927	5.240E 05	0.69068E-01
34.96	0.57	0.604	.7173	.0542	.0961	5.361E 05	0.34343E-01

BODY NUMBER=1

BODY DEPTH=2

VELOCITY(KTS)=0.75

X(INCH)	RADUIS	CORR. RADIUS	DELTA	DELTA-STAR	THETA	REYNOLDS NO.	Y-NORM/
0.17	0.37	0.371	.0152	.0019	.0015	1.295E 03	0.23524E-01
0.87	0.88	0.886	.0559	.0067	.0055	6.626E 03	0.56149E-01
2.12	1.30	1.309	.1134	.0134	.0113	1.615E 04	0.82974E-01
3.85	1.60	1.621	.1815	.0211	.0182	2.932E 04	0.10272E-00
6.02	1.81	1.839	.2576	.0295	.0261	4.585E 04	0.11656E-00
8.53	1.96	1.998	.3379	.0380	.0346	6.497E 04	0.12661E-00
11.31	2.00	2.046	.4195	.0462	.0433	8.614E 04	0.12967E-00
14.25	2.00	2.054	.4997	.0539	.0522	1.085E 05	0.13016E-00
17.24	2.00	2.061	.5765	.0610	.0609	1.313E 05	0.13061E-00
20.19	2.00	2.067	.6484	.0674	.0692	1.538E 05	0.13101E-00
22.96	2.00	2.073	.7131	.0729	.0767	1.749E 05	0.13137E-00
25.48	2.00	2.078	.7699	.0777	.0835	1.941E 05	0.13167E-00
27.65	2.00	2.082	.8173	.0816	.0892	2.106E 05	0.13191E-00
29.38	2.00	2.085	.8543	.0846	.0937	2.238E 05	0.13210E-00
30.63	1.63	1.697	.8628	.0818	.0972	2.333E 05	0.10754E-00
31.33	0.78	0.805	.7922	.0637	.1005	2.386E 05	0.50993E-01

BODY NUMBER=3

BODY DEPTH=2

VELOCITY(KTS)=0.75

X(INCH)	RADUIS	CORR. RADIUS	DELTA	DELTA-STAR	THETA	REYNOLDS NO.	Y-NORM/
0.19	0.40	0.401	.0167	.0020	.0016	1.447E 03	0.22831E-01
0.97	0.94	0.947	.0610	.0073	.0060	7.388E 03	0.53850E-01
2.36	1.37	1.384	.1234	.0146	.0123	1.797E 04	0.78741E-01
4.30	1.67	1.693	.1980	.0230	.0199	3.275E 04	0.96293E-01
6.72	1.87	1.902	.2808	.0320	.0285	5.118E 04	0.10819E-00
9.53	1.97	2.011	.3679	.0410	.0378	7.258E 04	0.11439E-00
12.62	2.00	2.050	.4557	.0497	.0474	9.612E 04	0.11659E-00
15.90	2.00	2.058	.5426	.0579	.0570	1.211E 05	0.11706E-00
19.24	2.00	2.065	.6256	.0654	.0665	1.465E 05	0.11748E-00
22.52	2.00	2.072	.7030	.0721	.0756	1.715E 05	0.11787E-00
25.62	2.00	2.078	.7730	.0780	.0839	1.951E 05	0.11820E-00
28.43	2.00	2.083	.8340	.0830	.0912	2.165E 05	0.11849E-00
30.85	1.94	2.026	.8826	.0863	.0975	2.350E 05	0.11524E-00
32.79	1.62	1.702	.9051	.0848	.1027	2.497E 05	0.96797E-01
34.17	1.15	1.220	.8923	.0772	.1069	2.603E 05	0.69414E-01
34.96	0.57	0.606	.8028	.0586	.1110	2.663E 05	0.34498E-01

BODY NUMBER=5

BODY DEPTH=3

VELOCITY(KTS)=0.75

X(INCH)	RADUIS	CORR. RADIUS	DELTA	DELTA-STAR	THETA	REYNOLDS NO.	Y-NORM/
0.22	0.42	0.422	.0187	.0023	.0018	1.676E 03	0.20604E-01
1.13	1.00	1.008	.0689	.0082	.0068	8.606E 03	0.49250E-01
2.75	1.42	1.436	.1392	.0163	.0139	2.094E 04	0.70191E-01
5.00	1.72	1.746	.2228	.0257	.0225	3.808E 04	0.85316E-01
7.81	1.91	1.946	.3155	.0356	.0322	5.948E 04	0.95092E-01
11.08	2.00	2.046	.4130	.0456	.0426	8.439E 04	0.99979E-01
14.69	2.00	2.055	.5113	.0550	.0535	1.119E 05	0.10044E-00
18.50	2.00	2.064	.6076	.0638	.0645	1.409E 05	0.10087E-00
22.39	2.00	2.072	.7000	.0718	.0752	1.705E 05	0.10126E-00
26.20	2.00	2.079	.7857	.0790	.0854	1.995E 05	0.10161E-00
29.81	1.98	2.065	.8626	.0851	.0948	2.270E 05	0.10093E-00
33.08	1.85	1.938	.9239	.0887	.1033	2.519E 05	0.94742E-01
35.89	1.57	1.657	.9614	.0882	.1106	2.734E 05	0.81000E-01
38.14	1.18	1.260	.9655	.0824	.1169	2.905E 05	0.61602E-01
39.75	0.73	0.795	.9154	.0692	.1225	3.027E 05	0.38848E-01
40.67	0.28	0.316	.7428	.0443	.1297	3.098E 05	0.15430E-01

TABLE G-II - SAMPLES OF COMPUTER OUTPUT, PROGRAM III

BODY NUMBER=1

DEPTH=2

SPEED=0.75

X(I)	Y(I)	U(I)	P(I)	PCC(I)	VEL(I)/
-0.98940E 00	0.23524E-01	0.66402E 00	0.55907E 00	0.52739E 02	0.49802E-00
-0.94458E 00	0.56149E-01	0.98608E 00	0.27646E-01	0.51912E 02	0.73956E 00
-0.86563E 00	0.82974E-01	0.74893E 00	0.43910E-00	0.52552E 02	0.56170E 00
-0.75540E 00	0.10272E-00	0.10463E 01	-0.94643E-01	0.51722E 02	0.78469E 00
-0.61788E 00	0.11656E-00	0.10358E 01	-0.72811E-01	0.51756E 02	0.77682E 00
-0.45802E-00	0.12661E-00	0.10413E 01	-0.84395E-01	0.51738E 02	0.78101E 00
-0.28160E-00	0.12967E-00	0.10222E 01	-0.44932E-01	0.51799E 02	0.76666E 00
-0.95013E-01	0.13016E-00	0.10106E 01	-0.21251E-01	0.51836E 02	0.75793E 00
0.95013E-01	0.13061E-00	0.10090E 01	-0.17995E-01	0.51841E 02	0.75672E 00
0.28160E-00	0.13101E-00	0.10099E 01	-0.19858E-01	0.51838E 02	0.75741E 00
0.45802E-00	0.13137E-00	0.10136E 01	-0.27446E-01	0.51826E 02	0.76022E 00
0.61788E 00	0.13167E-00	0.10200E 01	-0.40472E-01	0.51806E 02	0.76503E 00
0.75540E 00	0.13191E-00	0.10552E 01	-0.11343E-00	0.51692E 02	0.79140E 00
0.86563E 00	0.13210E-00	-0.12431E 01	-0.54533E 00	0.51020E 02	0.93233E 00
0.94458E 00	0.10754E-00	0.11424E 01	-0.30503E-00	0.51394E 02	0.85678E 00
0.98940E 00	0.50993E-01	0.55872E 00	0.68783E 00	0.52939E 02	0.41904E-00

BODY NUMBER=3

DEPTH=2

SPEED=0.75

X(I)	Y(I)	U(I)	P(I)	PCC(I)	VEL(I)/
-0.98940E 00	0.22831E-01	0.70115E 00	0.50839E 00	0.52660E 02	0.52586E 00
-0.94458E 00	0.53850E-01	0.10042E 01	-0.85096E-02	0.51856E 02	0.75318E 00
-0.86563E 00	0.78741E-01	0.10542E 01	-0.11125E-00	0.51696E 02	0.79062E 00
-0.75540E 00	0.96293E-01	0.10473E 01	-0.96933E-01	0.51718E 02	0.78551E 00
-0.61788E 00	0.10819E-00	0.10410E 01	-0.83723E-01	0.51739E 02	0.78077E 00
-0.45802E-00	0.11439E-00	0.10281E 01	-0.56907E-01	0.51780E 02	0.77104E 00
-0.28160E-00	0.11659E-00	0.10166E 01	-0.33406E-01	0.51817E 02	0.76242E 00
-0.95013E-01	0.11706E-00	0.10088E 01	-0.17689E-01	0.51841E 02	0.75660E 00
0.95013E-01	0.11748E-00	0.10081E 01	-0.16231E-01	0.51844E 02	0.75606E 00
0.28160E-00	0.11787E-00	0.10123E 01	-0.24782E-01	0.51830E 02	0.75924E 00
0.45802E-00	0.11820E-00	0.10082E 01	-0.16448E-01	0.51843E 02	0.75614E 00
0.61788E 00	0.11849E-00	0.10435E 01	-0.88884E-01	0.51731E 02	0.78262E 00
0.75540E 00	0.11524E-00	0.11069E 01	-0.22517E-00	0.51518E 02	0.83016E 00
0.86563E 00	0.96797E-01	0.10737E 01	-0.15292E-00	0.51631E 02	0.80531E 00
0.94458E 00	0.69414E-01	0.10298E 01	-0.60430E-01	0.51775E 02	0.77233E 00
0.98940E 00	0.34498E-01	0.77644E 00	0.39714E-00	0.52487E 02	0.58233E 00

BODY NUMBER=3

DEPTH=1

SPEED=1.12

X(I)	Y(I)	U(I)	P(I)	PCC(I)	VEL(I)/
-0.98940E 00	0.22825E-01	0.70131E 00	0.50816E 00	0.95133E 02	0.78547E 00
-0.94458E 00	0.53822E-01	0.10043E 01	-0.86126E-02	0.93340E 02	0.11248E 01
-0.86563E 00	0.78683E-01	0.10542E 01	-0.11126E-00	0.92984E 02	0.11807E 01
-0.75540E 00	0.96202E-01	0.10473E 01	-0.96911E-01	0.93033E 02	0.11730E 01
-0.61788E 00	0.10806E-00	0.10409E 01	-0.83487E-01	0.93080E 02	0.11658E 01
-0.45802E-00	0.11424E-00	0.10280E 01	-0.56869E-01	0.93172E 02	0.11514E 01
-0.28160E-00	0.11641E-00	0.10165E 01	-0.33273E-01	0.93254E 02	0.11385E 01
-0.95013E-01	0.11685E-00	0.10087E 01	-0.17421E-01	0.93309E 02	0.11297E 01
0.95013E-01	0.11725E-00	0.10079E 01	-0.15789E-01	0.93315E 02	0.11288E 01
0.28160E-00	0.11762E-00	0.10096E 01	-0.19289E-01	0.93303E 02	0.11307E 01
0.45802E-00	0.11794E-00	0.10149E 01	-0.29985E-01	0.93266E 02	0.11367E 01
0.61788E 00	0.11821E-00	0.10399E 01	-0.81449E-01	0.93087E 02	0.11647E 01
0.75540E 00	0.11497E-00	0.11064E 01	-0.22402E-00	0.92592E 02	0.12391E 01
0.86563E 00	0.96544E-01	0.10732E 01	-0.15169E-00	0.92843E 02	0.12019E 01
0.94458E 00	0.69213E-01	0.10289E 01	-0.58731E-01	0.93166E 02	0.11524E 01
0.98940E 00	0.34408E-01	0.77605E 00	0.39775E-00	0.94750E 02	0.86917E 00

BODY NUMBER=3

DEPTH=2

SPEED=1.51

X(I)	Y(I)	U(I)	P(I)	PCC(I)	VEL(I)/
-0.98940E 00	0.22821E-01	0.70143E 00	0.50799E 00	0.55072E 02	0.10592E 01
-0.94458E 00	0.53803E-01	0.10043E 01	-0.87155E-02	0.51814E 02	0.15166E 01
-0.86563E 00	0.78642E-01	0.10542E 01	-0.11127E-00	0.51167E 02	0.15918E 01
-0.75540E 00	0.96138E-01	0.10473E 01	-0.96905E-01	0.51258E 02	0.15815E 01
-0.61788E 00	0.10797E-00	0.10409E 01	-0.83397E-01	0.51343E 02	0.15717E 01
-0.45802E-00	0.11413E-00	0.10280E 01	-0.56824E-01	0.51510E 02	0.15523E 01
-0.28160E-00	0.11628E-00	0.10165E 01	-0.33229E-01	0.51659E 02	0.15349E 01
-0.95013E-01	0.11670E-00	0.10086E 01	-0.17329E-01	0.51760E 02	0.15230E 01
0.95013E-01	0.11709E-00	0.10079E 01	-0.15799E-01	0.51769E 02	0.15219E 01
0.28160E-00	0.11744E-00	0.10095E 01	-0.19173E-01	0.51748E 02	0.15244E 01
0.45802E-00	0.11775E-00	0.10148E 01	-0.29892E-01	0.51680E 02	0.15324E 01
0.61788E 00	0.11801E-00	0.10398E 01	-0.81180E-01	0.51357E 02	0.15701E 01
0.75540E 00	0.11477E-00	0.11062E 01	-0.22358E-00	0.50459E 02	0.16703E 01
0.86563E 00	0.96362E-01	0.10729E 01	-0.15105E-00	0.50916E 02	0.16200E 01
0.94458E 00	0.69068E-01	0.10284E 01	-0.57650E-01	0.51505E 02	0.15529E 01
0.98940E 00	0.34343E-01	0.77580E 00	0.39813E-00	0.54379E 02	0.11715E 01

BODY NUMBER=5

DEPTH=3

SPEED=0.75

X(I)	Y(I)	U(I)	P(I)	PCC(I)	VEL(I)/
-0.98940E 00	0.20604E-01	0.70371E 00	0.50479E 00	0.19462E 02	0.52778E 00
-0.94458E 00	0.49250E-01	0.10285E 01	-0.57780E-01	0.18587E 02	0.77136E 00
-0.86563E 00	0.70191E-01	0.10469E 01	-0.96035E-01	0.18527E 02	0.78519E 00
-0.75540E 00	0.85316E-01	0.10435E 01	-0.88918E-01	0.18538E 02	0.78263E 00
-0.61788E 00	0.95092E-01	0.10351E 01	-0.71388E-01	0.18566E 02	0.77631E 00
-0.45802E-00	0.99979E-01	0.10267E 01	-0.54101E-01	0.18593E 02	0.77002E 00
-0.28160E-00	0.10044E-00	0.10093E 01	-0.18611E-01	0.18648E 02	0.75695E 00
-0.95013E-01	0.10087E-00	0.10071E 01	-0.14236E-01	0.18655E 02	0.75532E 00
0.95013E-01	0.10126E-00	0.10076E 01	-0.15212E-01	0.18653E 02	0.75568E 00
0.28160E-00	0.10161E-00	0.10133E 01	-0.26690E-01	0.18635E 02	0.76994E 00
0.45802E-00	0.10093E-00	0.10309E 01	-0.62655E-01	0.18579E 02	0.77314E 00
0.61788E 00	0.94742E-01	0.10432E 01	-0.88368E-01	0.18539E 02	0.78244E 00
0.75540E 00	0.81000E-01	0.10346E 01	-0.70363E-01	0.18567E 02	0.77594E 00
0.86563E 00	0.61602E-01	0.10135E 01	-0.27248E-01	0.18634E 02	0.76015E 00
0.94458E 00	0.38848E-01	0.95810E 00	0.82038E-01	0.18804E 02	0.71858E 00
0.98940E 00	0.15430E-01	0.77138E 00	0.40498E-00	0.19307E 02	0.57853E 00

APPENDIX H - LITERATURE CITATIONS

1. H. E. Saunders, Hydrodynamics in Ship Design, Vol.II, Society of Naval Architects and Marine Engineers, New York, 1956, pp. 133-135.

2. B. S. Stratford, "Prediction of Separation of Turbulent Boundary Layers," Journal of Fluid Mechanics, Vol.5,Pt.I., January, 1959, pp. 1-16.

3. Society of Naval Architects and Marine Engineers, Panel H-11 (Flow Studies), Minutes of meeting No. 9, 13, May,1959, p. 8.

4. H. Eckert, "Simplified Treatment of the Turbulent Boundary Layer along a Cylinder in Compressible Flow," Journal of Aeronautical Sciences, Vol.19, No.1, January,1952,pp.23-28.

5. Y. S. Yu, "Effect of Transverse Curvature on Turbulent Boundary Layer Characteristics," Journal of Ship Research, Vol.2, No.3, December, 1958, pp.33-51.

6. L. Landweber, "Effect of Transverse Curvature on Frictional Resistance," David Taylor Model Basin Report 689,March,1949.

7. P. S. Granville "The Calculation of the Viscous Drag of Bodies of Revolution," David Taylor Model Basin Report 849, July, 1953, pp.5-6

8. L. Landweber, "The Axially Symmetric Potential Flow about Elongated Bodies of Revolution," David Taylor Model Basin Report 761, August, 1951.

9. H. Rouse, Elementary Mechanics of Fluids, Wiley and Sons, New York, 1946.

10. S. F. Hoerner, Fluid-Dynamic Drag, Author, New York, 1957.

Although not specifically cited the following references were very useful in the thesis work as background and source references.

A. H. E. Saunders, Hydrodynamics in Ship Design, Vols. I and II, Chapters 7, 23, and 46, Society of Naval Architects and Marine Engineers, New York, 1956.

B. H. Schlichting, Boundary Layer Theory, First English Edition, McGraw Hill, New York, 1955.

C. F. H. Todd, "Fundamentals of Ship Model Testing," Society of Naval Architects and Marine Engineers Transactions, Vol. 59, 1951, pp.850-896